# Application of anelastic and compressible EULAG solvers for limited-area numerical weather prediction in the COSMO consortium

Damian K. Wójcik, Zbigniew P. Piotrowski, Bogdan Rosa
and Michał Z. Ziemiański

Institute of Meteorology and Water Management
National Research Institute
Warsaw, Poland

ECMWF, Reading, 4th October 2016

# Outline

1. Introduction

2. Anelastic COSMO-EULAG
    a. Surface and upper-air verification scores of weather forecasts
    b. Test at high resolution

3. Compressible COSMO-EULAG
    a. Idealized tests:
        - Cold density current
        - Channel flows
        - Orographic flows

# Introduction

Two Priority Projects of COSMO consortium (CDC, CELO) resulted in the development of a nonhydrostatic limited-area COSMO-EULAG model that is based on the anelastic set of equations and numerics adopted from the EULAG solver.

The new model is capable to provide competitive weather forecast with respect to the operational COSMO model (without data assimilation).

Since the development of compressible EULAG solver the priority of the COSMO consortium was shifted towards the compressible code (2015).

Following publication summarizes anelastic COSMO-EULAG model design and results for stably stratified flows (autumn weather):
*„Convection-permitting regional weather modeling with COSMO-EULAG: Compressible and anelastic solutions for a typical westerly flow over the Alps”*
Kurowski et. al., Monthly Weather Review, 2015.

# Introduction

Time integration of the EULAG is based on an unique combination of two numerical algorithms :

- Multidimensional positive definite advection transport algorithm (MPDATA)
- Preconditioned conjugate-residuals algorithm (GCRK) that solves elliptic Poisson equation arising from the anelastic mass divergence constraint

Time discretization scheme of the anelastic COSMO-EULAG follows the template :

$$\phi_{\mathrm{i}}^{n+1} = MPDATA_{\mathrm{i}}\left(\phi^{n} + \frac{\Delta t}{2}R^{n} + \Delta t F^{n}, \alpha^{n+1/2}, \phi_{bd}^{n}, G\right) + \frac{\Delta t}{2}R_{\mathrm{i}}^{n+1}$$

where R denotes dynamical terms (latent heat release as an option) and F denotes parameterization terms.

## Anelastic COSMO-EULAG

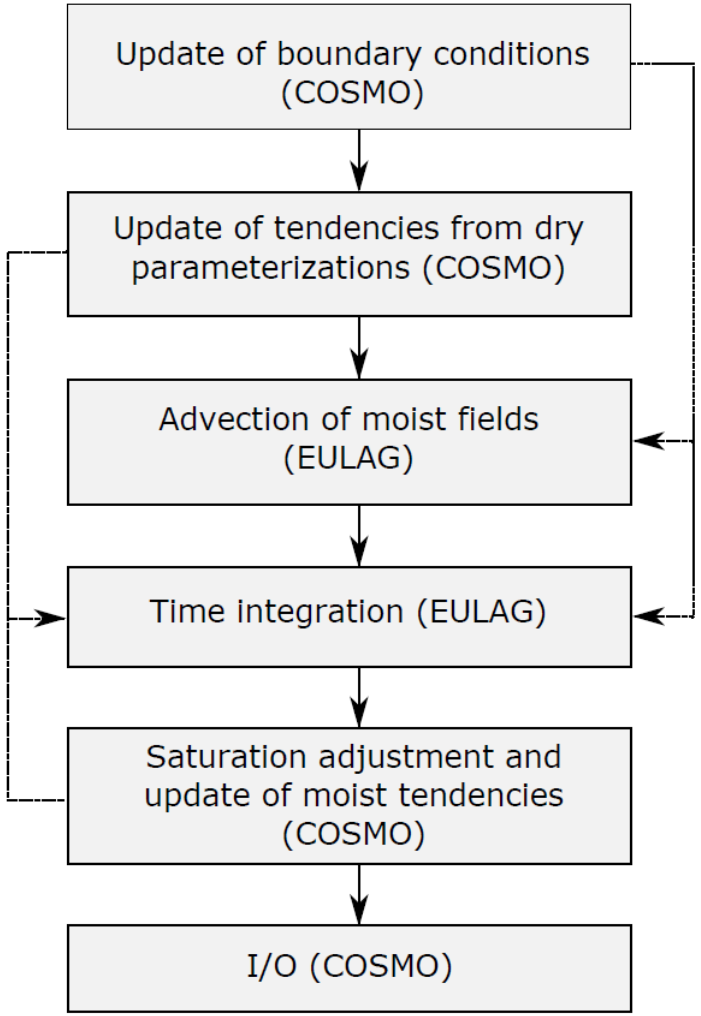

# Anelastic COSMO-EULAG

# Anelastic COSMO-EULAG: forecast verification

**Station network for surface verification:**

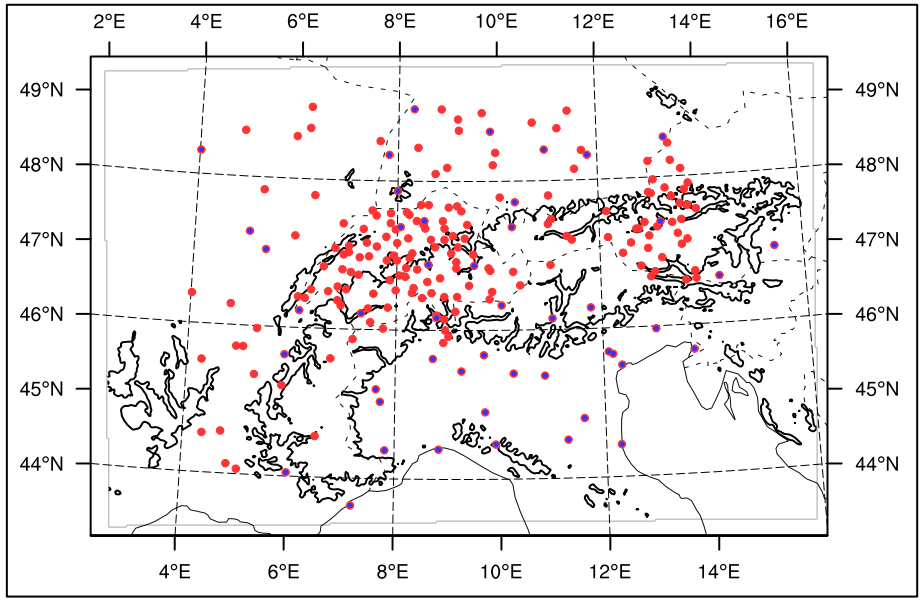


- 217 stations (Temperature, Rain…)
- 47 stations (TCC)

Two models are compared:

- COSMO with Runge-Kutta solver (default)
- Anelastic COSMO-EULAG

Verification covers two contrasting weather periods:

- 1-14 November 2013
- 1-14 June 2013

Next to the basic Gal-Chen coordinate system (with stretching) simulations with the SLEVE coordinates are performed.

SLEVE coordinate (see Schär et. al., 2002) employ a scale-dependent vertical decay of underlying terrain features. In COSMO implementation they become flat around 12km height.

**Station network for upper-air verification:**

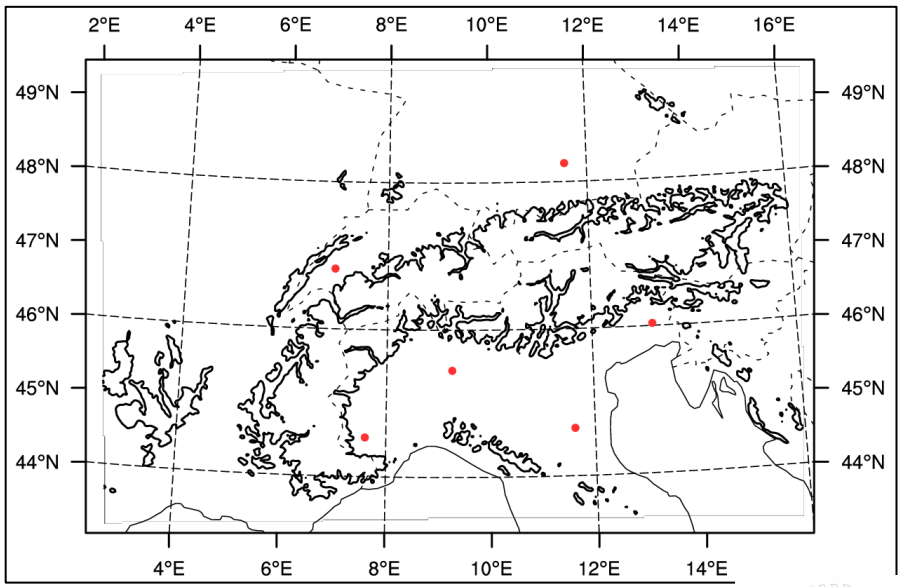


- 6 stations

# Surface verification: 1-14 November 2013

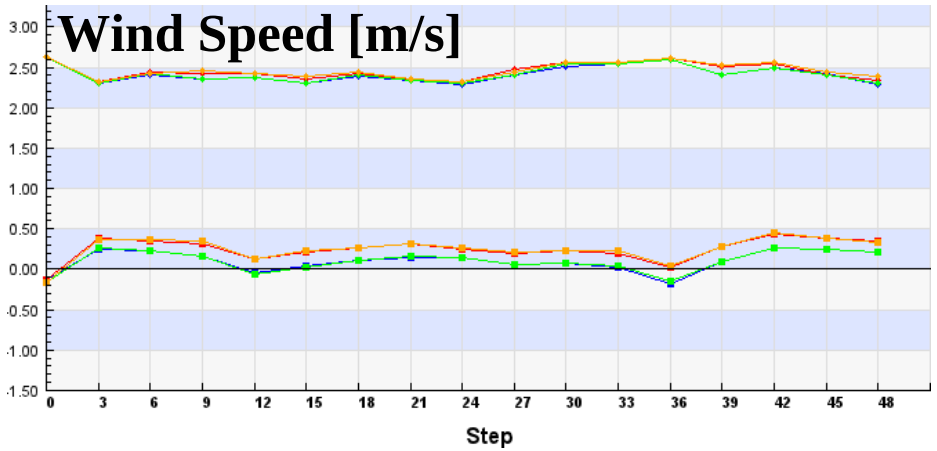


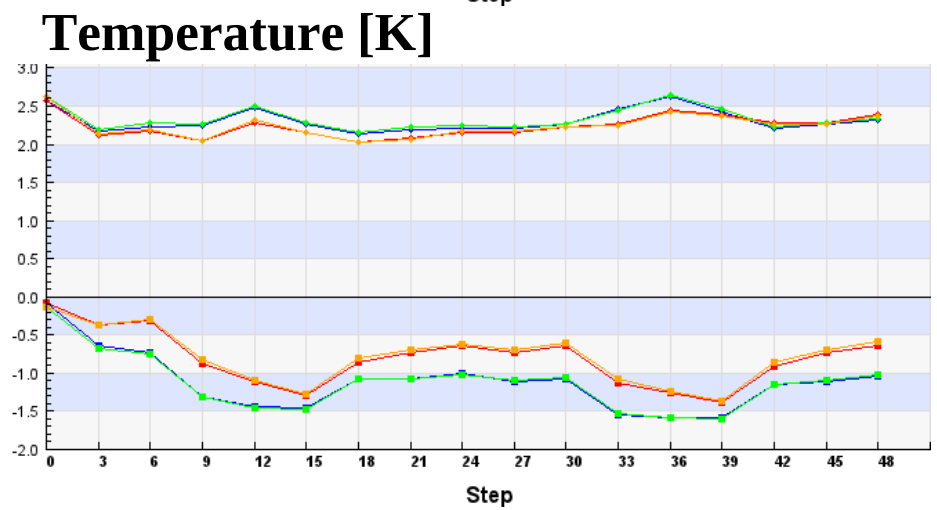


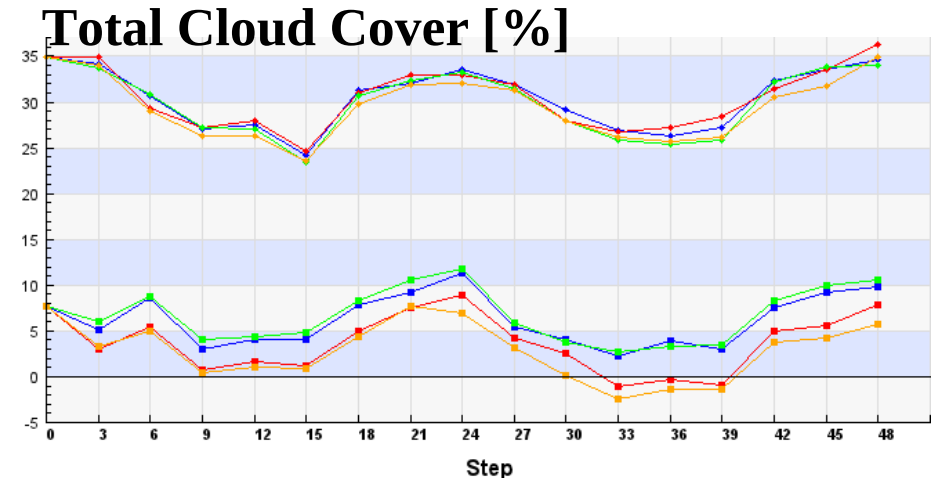


COSMO RK, Gal-Chen coords
COSMO RK, SLEVE coords
CE, Gal-Chen coords
CE, SLEVE coords

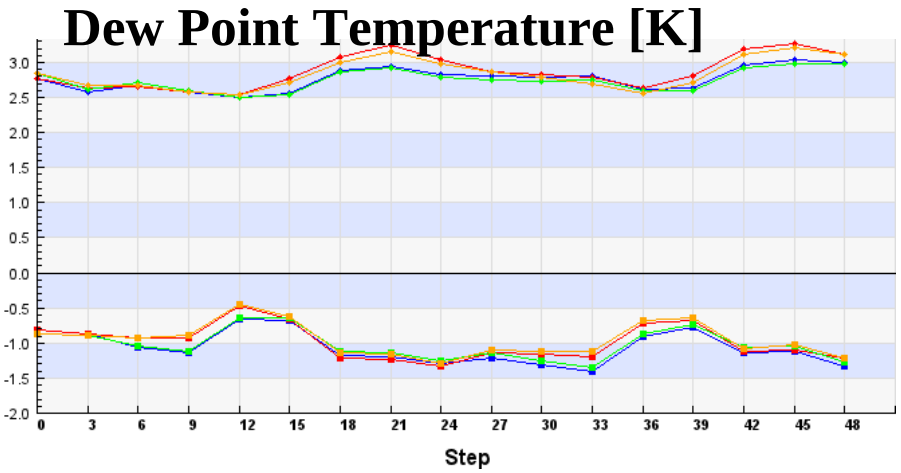


The usage of SLEEVE vertical coordinate system slightly improves the performance of both models in autumn weather conditions. In case of CE the biggest improvement is related to TCC.

# Upper-air verification: 1-14 Nov. 2013

COSMO RK, Gal-Chen coords
COSMO RK, SLEVE coords
CE, Gal-Chen coords
CE, SLEVE coords

## Upper-air Relative Humidity [K]

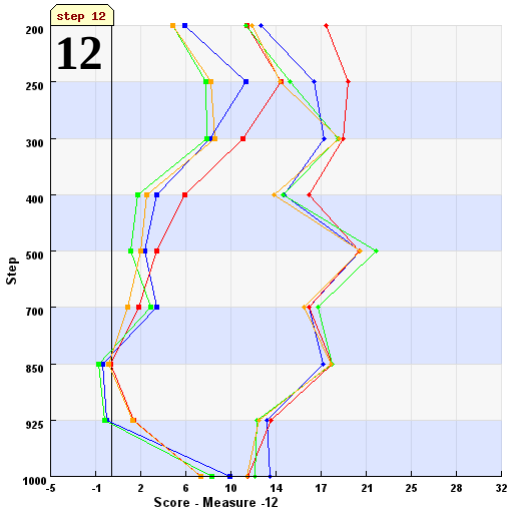


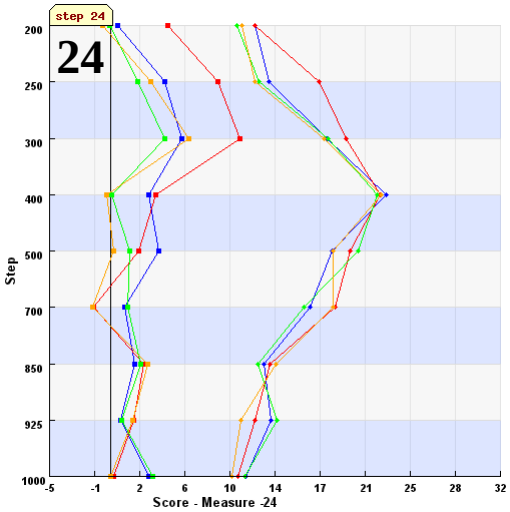


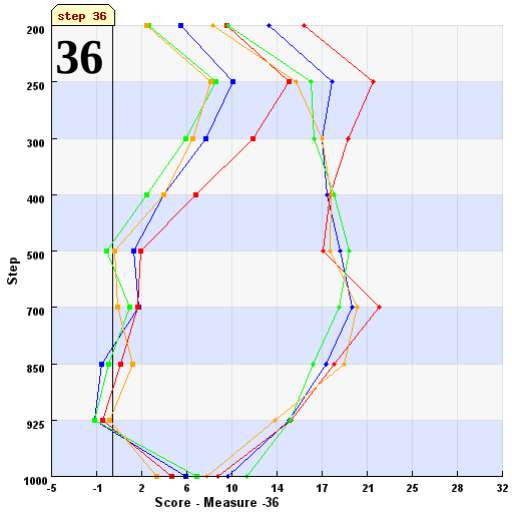


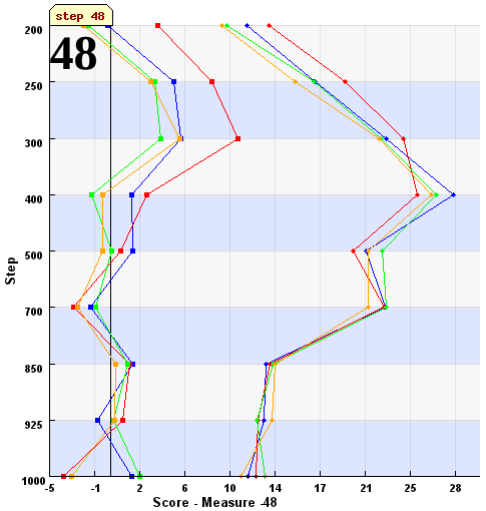


## Upper-air Temperature [K]

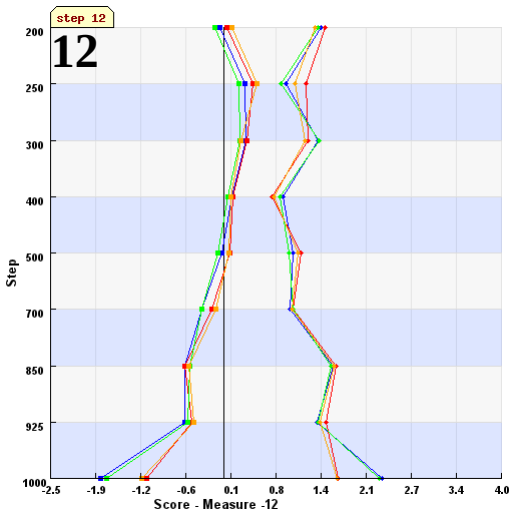


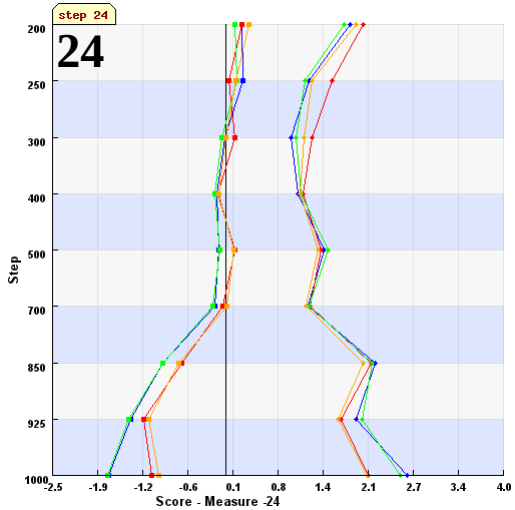


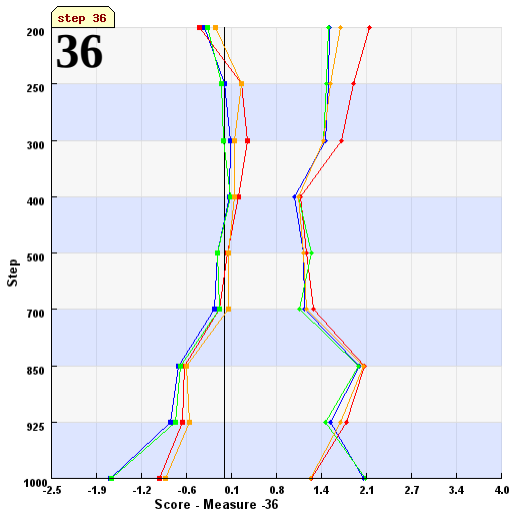


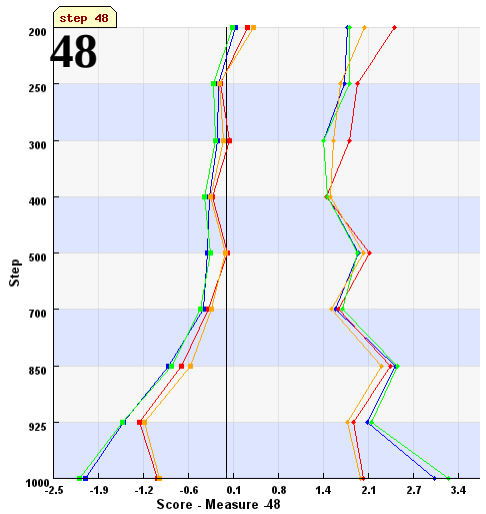


CE scores tend to improve when SLEVE coordinates are utilized.

# Surface verification: 1-14 June 2013

## Wind Speed [m/s]

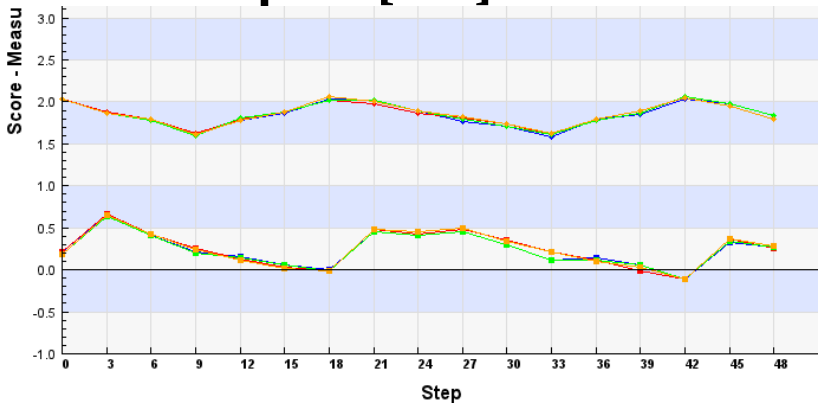


COSMO RK, Gal-Chen coords
COSMO RK, SLEVE coords
CE, Gal-Chen coords
CE, SLEVE coords

## Temperature [K]

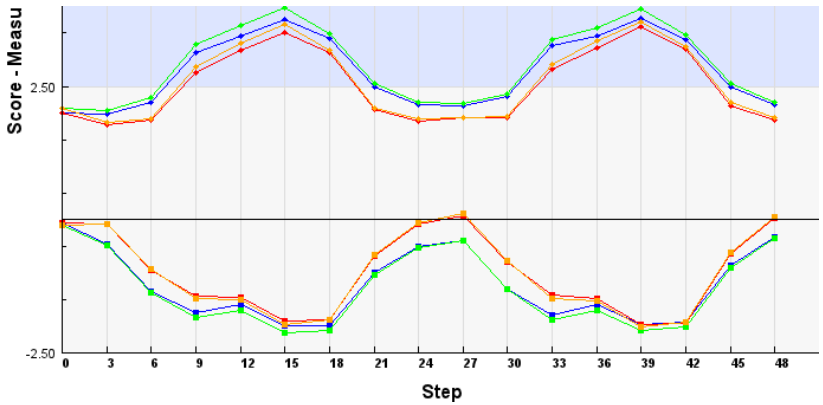


## Dew Point Temperature [K]

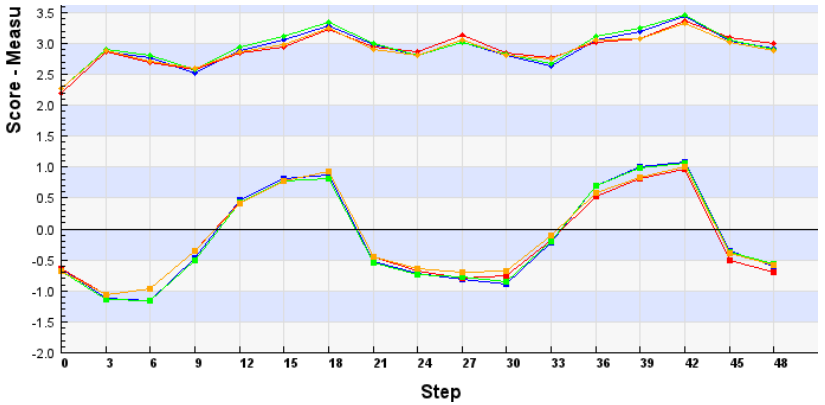


## Total Cloud Cover [%]

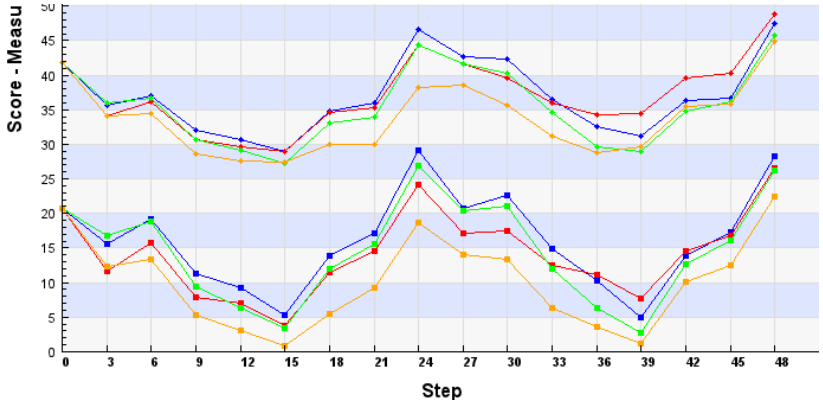


Periodicity in error magnitude is typical for summer and reflects the diurnal cycle of convection.

The usage of sleeve coordinates significantly improves TCC forecast scores of CE model.

# Upper-air verification: 1-14 June 2013

COSMO RK, Gal-Chen coords
COSMO RK, SLEVE coords
CE, Gal-Chen coords
CE, SLEVE coords

## Upper-air Relative Humidity [K]

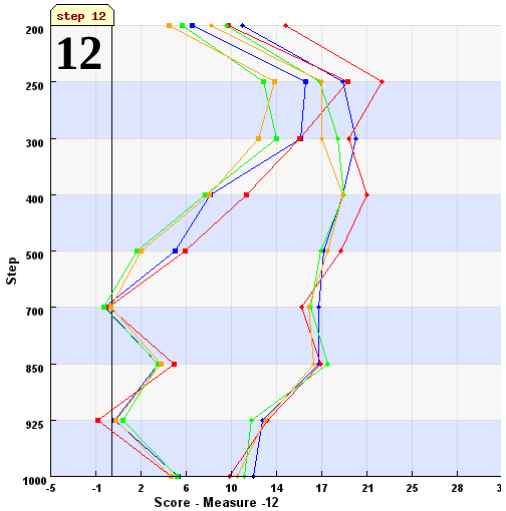


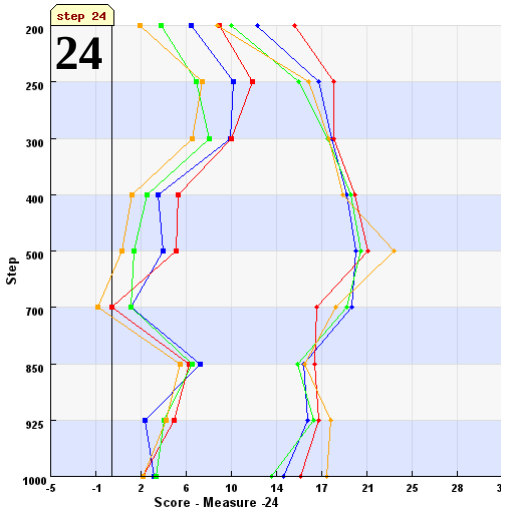


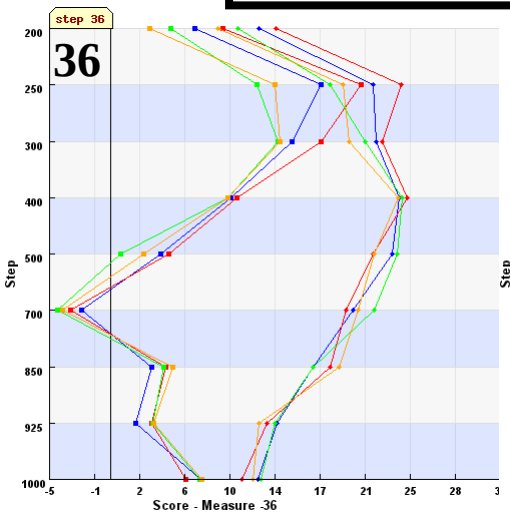


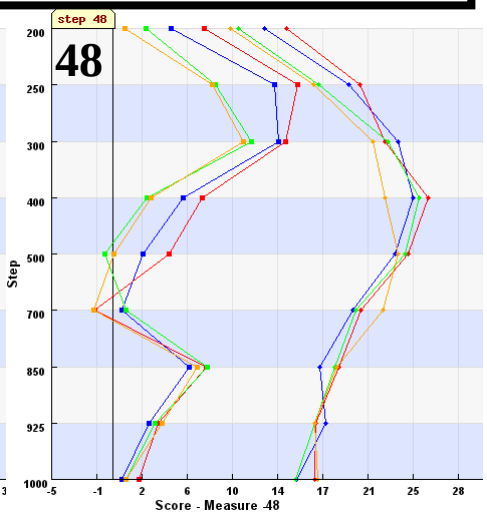


## Upper-air Temperature [K]

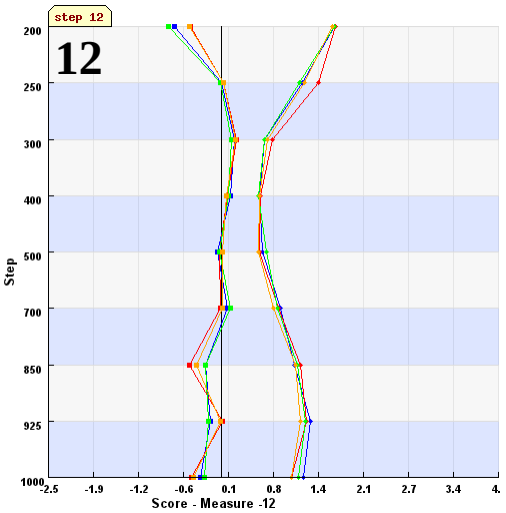


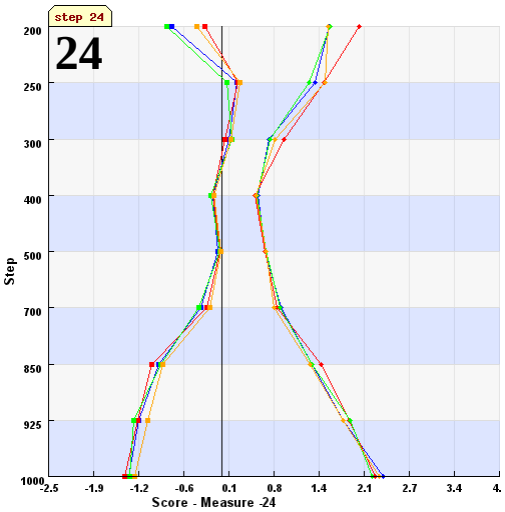


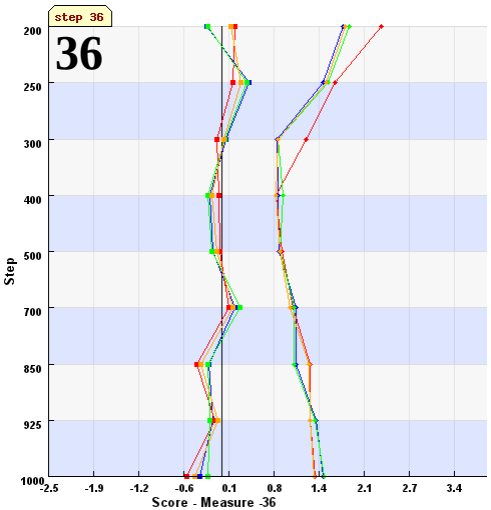


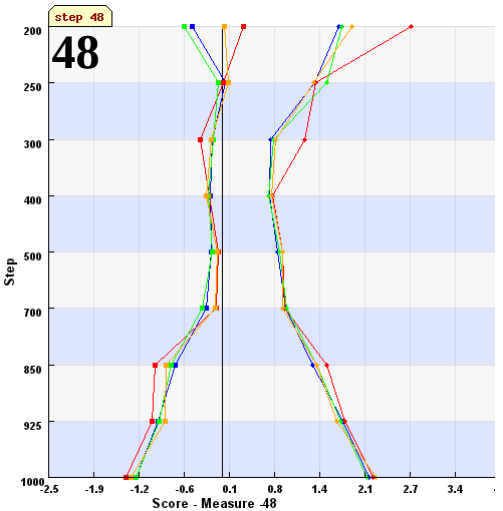


CE scores tend to improve when SLEVE coordinates are utilized.

# LES-type CE simulations in 100m horizontal grid size

The 2.2 km resolution CE weather forecast for the 19th July 2013 is used as a base for a LES-type CE simulations in 100 m horizontal grid size in a limited mountainous subdomain (see details in the table below, left). The new simulations starts at 6:00 UTC and last till 24:00 UTC.

The deep convective clouds formation at 15:00 UTC in the northern part of the computational domain (light blue rectangle) is shown in the MSG 10.8µm IR image (below, right). After 20:00 UTC the deep convection phase terminates.

| **Grid size** | **100 m** |
|---|---|
| WE x NS | 1860 x 1500 |
| Vertical levels | 61 |
| Domain height | ~23.5 km |
| Lateral absorber | 5.8 km |
| Sponge base height | 15 km |
| Initial and b.c. | CE 2.2 forecast |
| Forecast period | 18 hours, starting at 6:00 UTC |
| Turbulence param. | Smagorinsky-Lilly |
| The freq. of rad. coefficients calc. | 6 minutes |

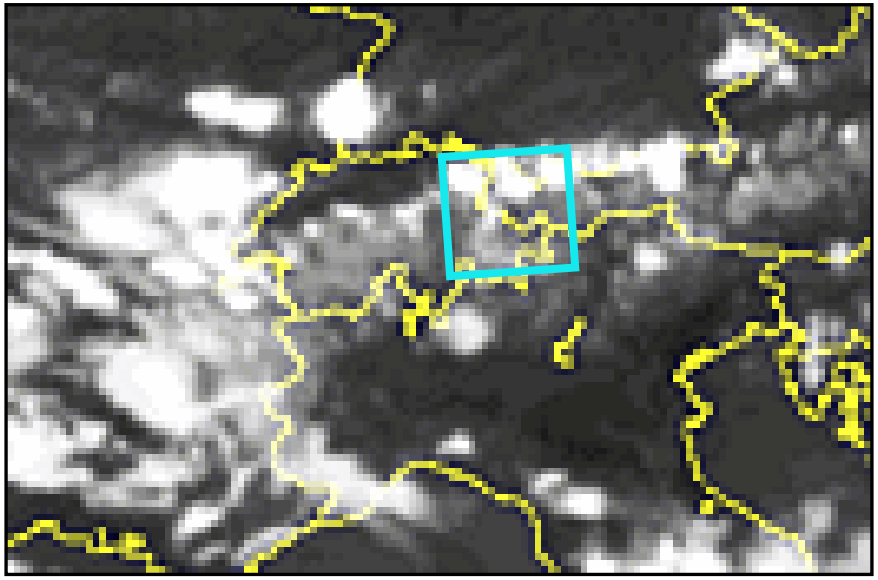

15:00 UTC, 19th July 2013

# Topography in LES type simulations

Two distinct topographies are used for LES type simulations :

1. Topography specific to 2.2 km grid size interpolated to 100 m grid (below, left)
2. Topography specific to 100 m grid size (below, middle)

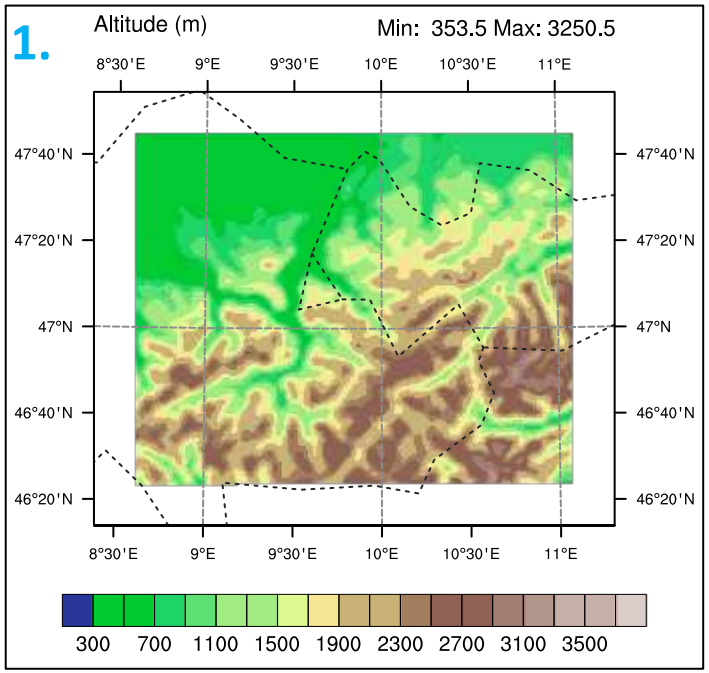


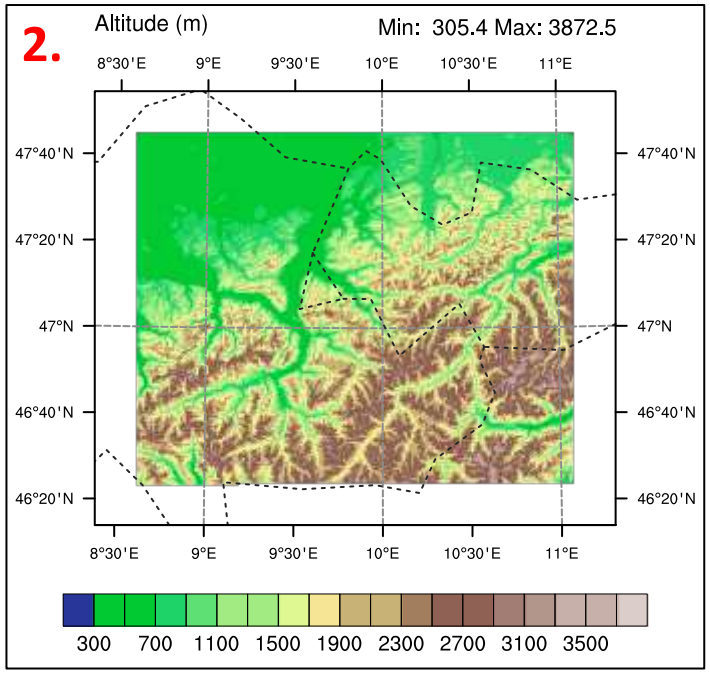


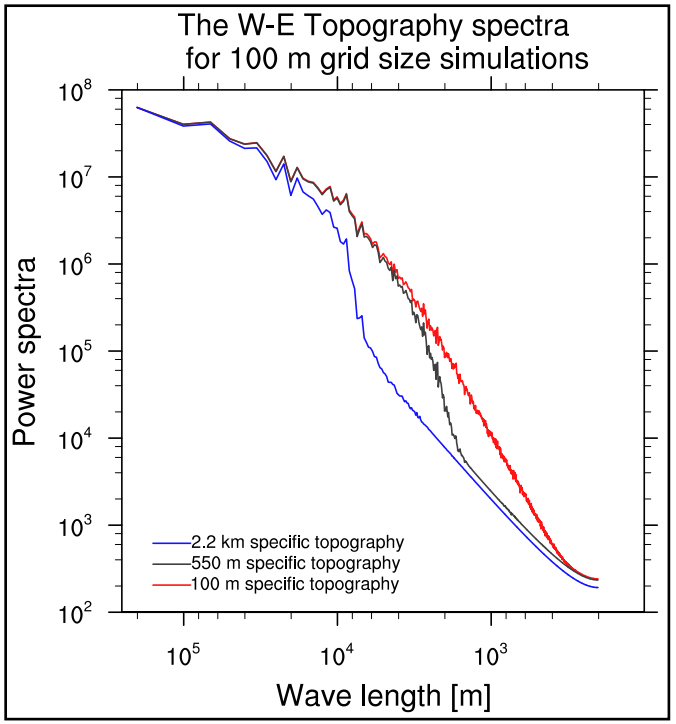

# Precipitation statistics

Spatial distribution of precipitation is generally similar for all simulations, but there are significant small scale differences. In the reference convection-permitting simulation the total precipitation amount is smaller comparing with LES simulations.

CE 2.2km, orography 2.2km

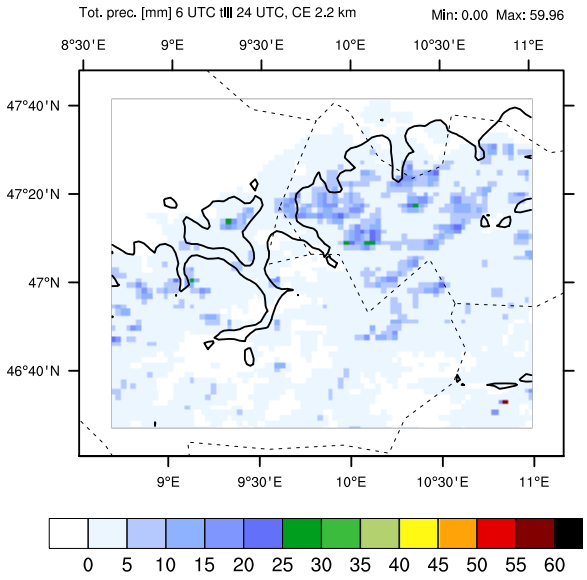


CE 100m, orography 2.2km

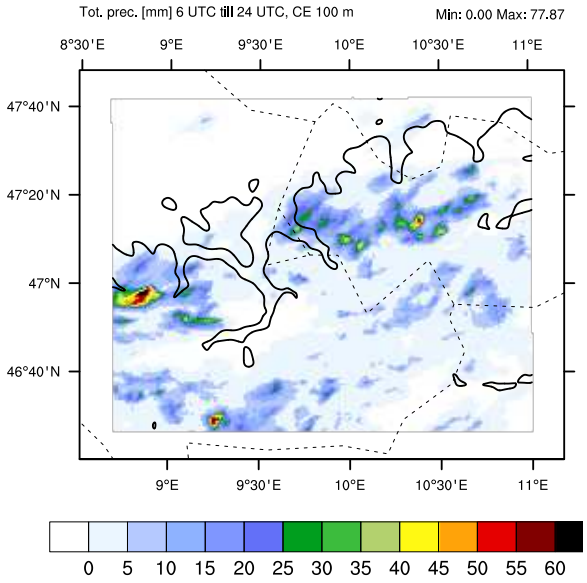


CE 100m, orography 100 m

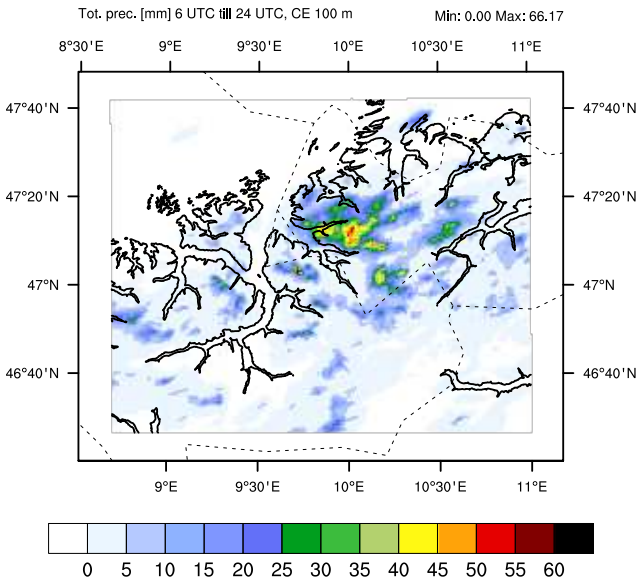


Total precipitation between 6 and 24 UTC

# Precipitation statistics

For LES studies introduction of realistic topography (100 m) resulted in later onset and earlier termination of deep convection, smaller precipitation amount and significant differences in flow pattern, especially in the lower tropospheric area (comparing to 2.2 km orography).

| **Total precip. from 6 till 24 UTC [kg/m²]** | |
|---|---|
| CE 2.2 km | 1.7 |
| CE 100 m with 2.2 km orography | 3.5 |
| CE 100 m with 100 m orography | 2.9 |

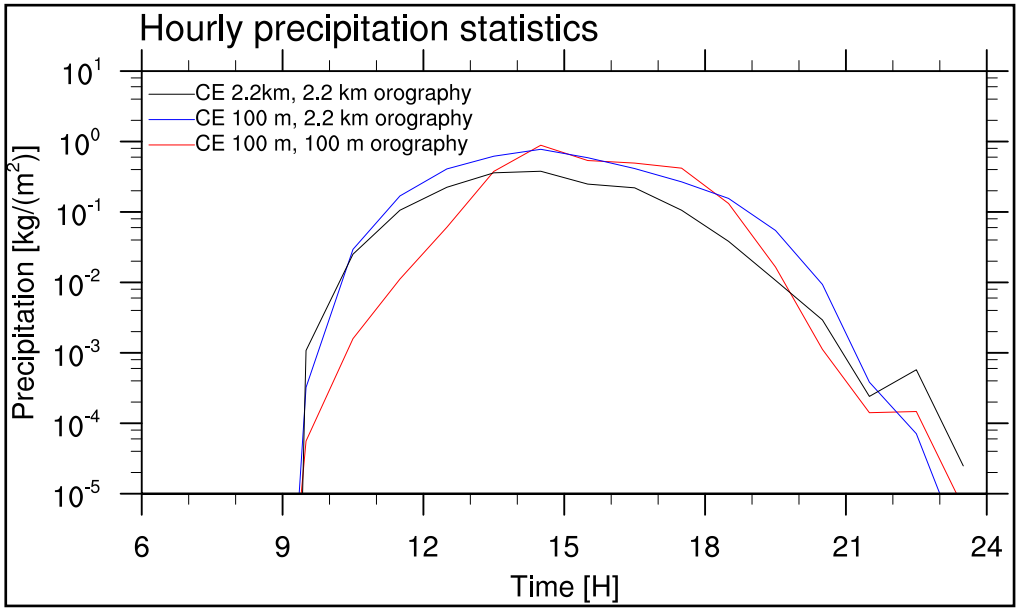


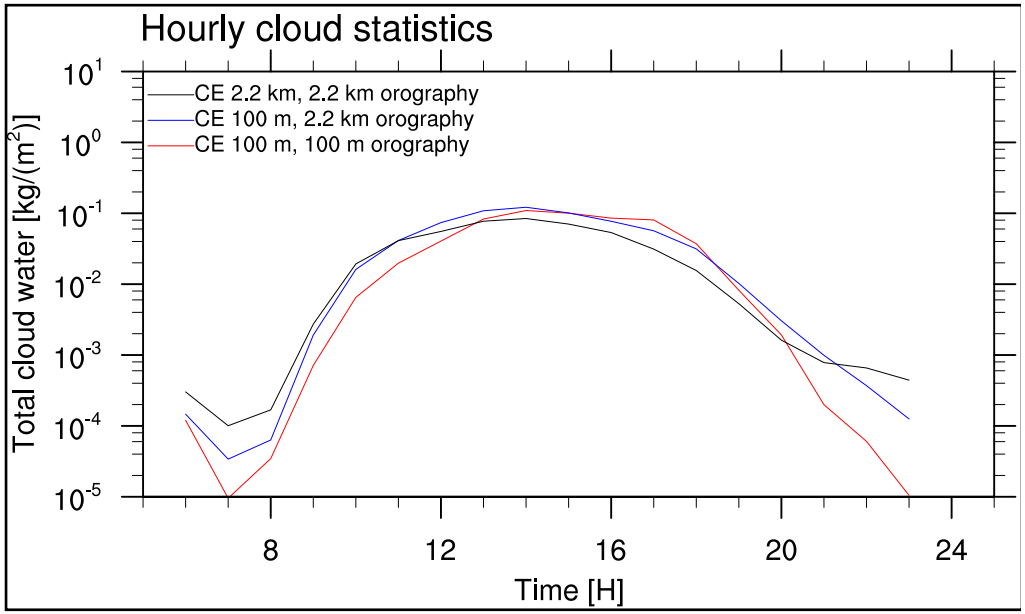

# Compressible COSMO-EULAG

# Cold density current

Straka, J. M., Wilhelmson, Robert B., Wicker, Louis J., Anderson, John R., Droegemeier, Kelvin K., Numerical solutions of a non-linear density current: A benchmark solution and comparison *International Journal for Numerical Methods in Fluids*, (**17)**, 1993

Experiment configuration:

- isentropic atmosphere, $\theta$ (z)=const (300K)
- open lateral boundaries
- free-slip bottom b.c.
- **constant subgrid mixing, K=75m²/s**
- domain size 51.2km x 6.4km
- bubble min. temperature -15K
- bubble size 8km × 4km
- no initial flow
- integration time 15 min
- isotropic grid

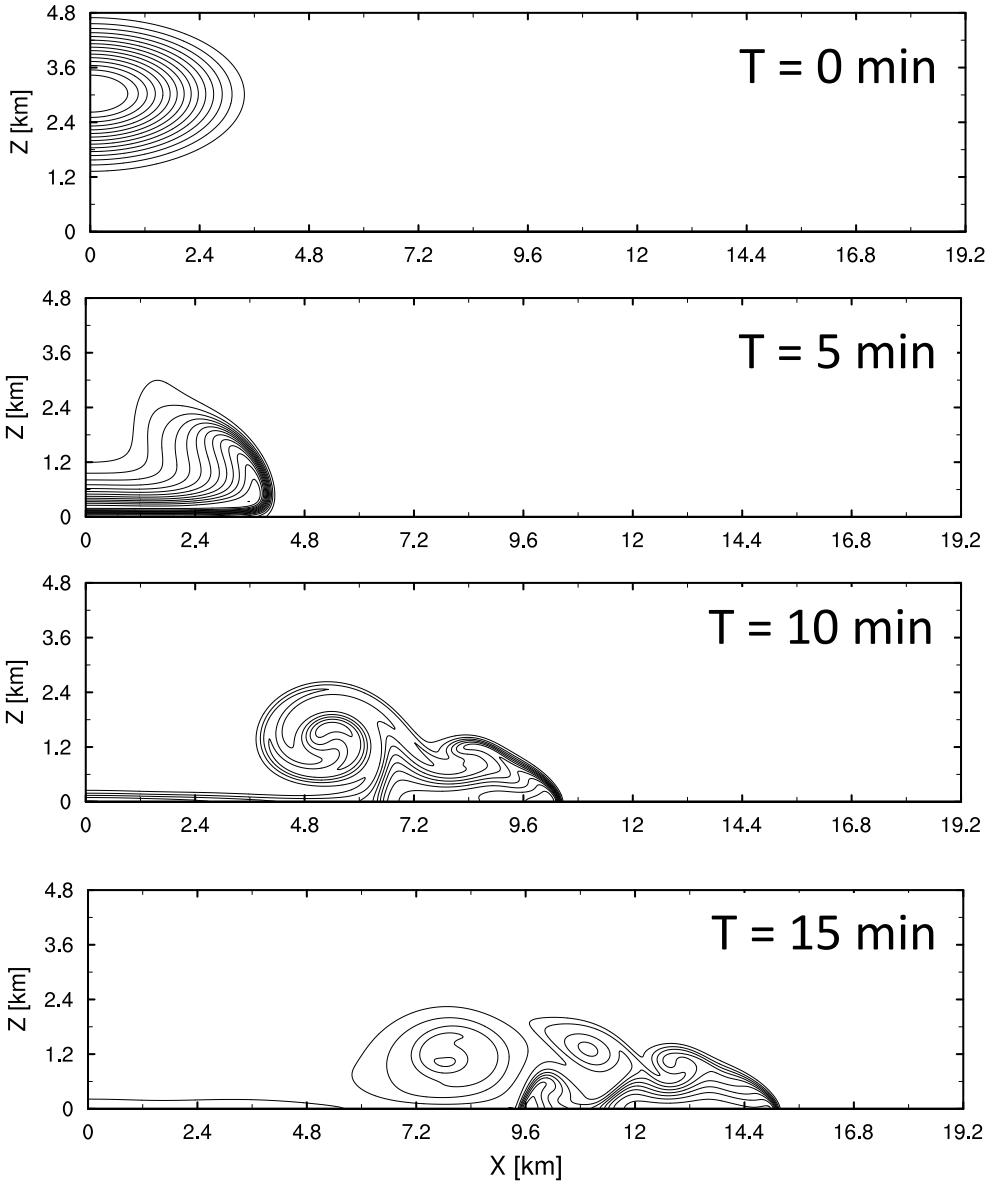


The solid isolines show potential temperature perturbation with respect to the isentropic atmosphere.

# Cold density current

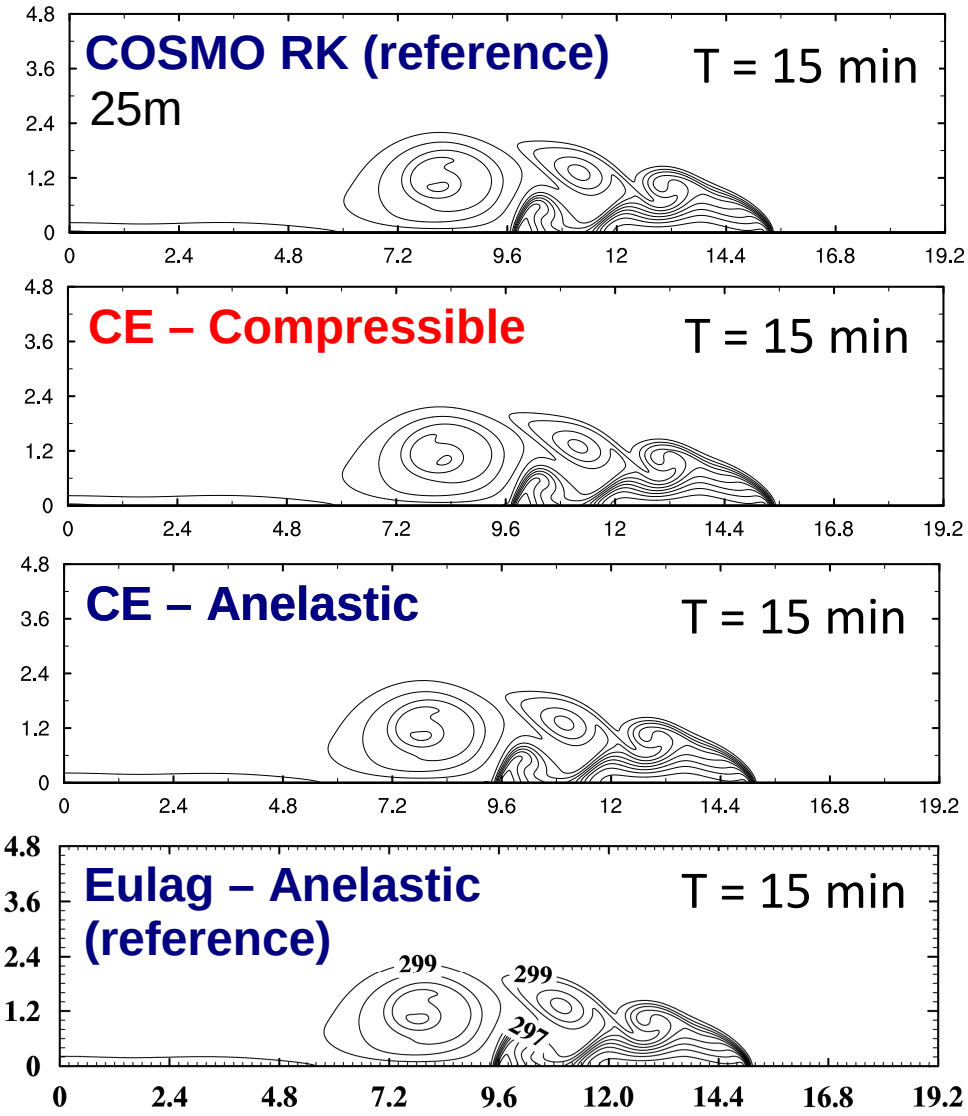


The sequence of figures confirms that the solutions obtained with 4 different models are in a qualitative agreement.

# Cold density current: P’ and W

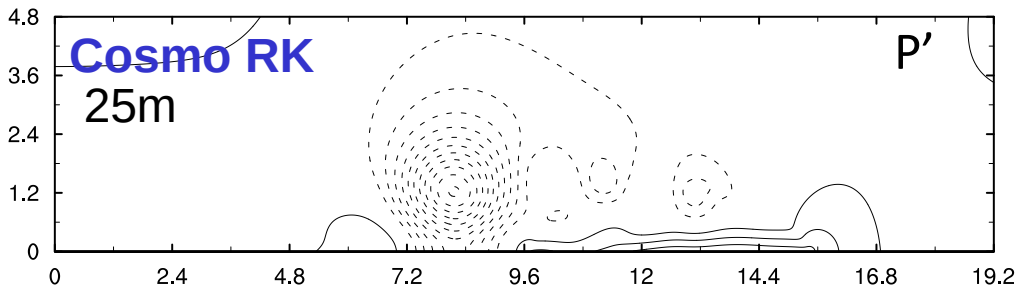


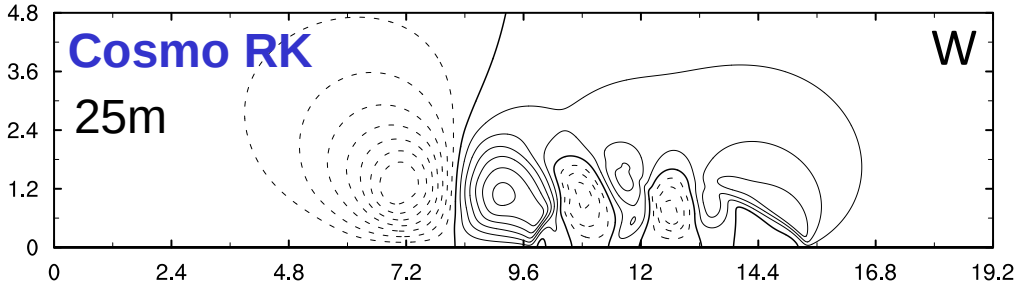


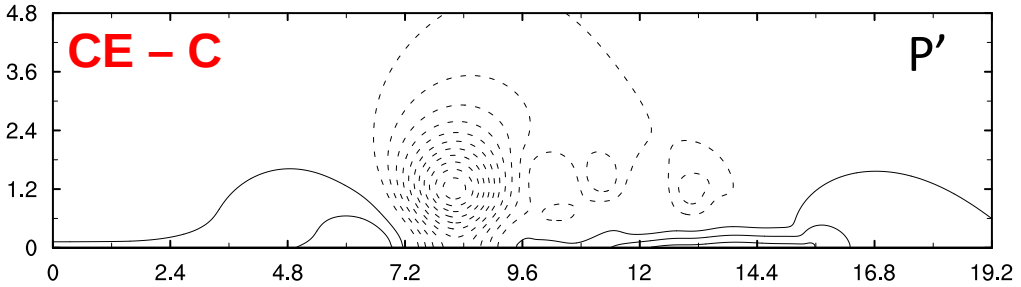


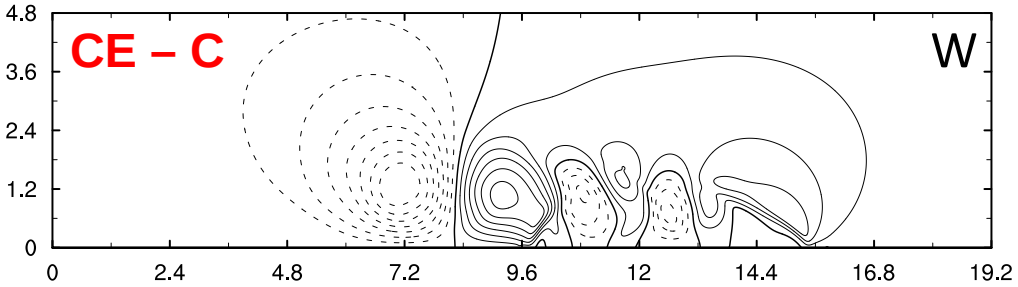


| Parameter | COSMO RK | | CE-C Implicit | |
|---|---|---|---|---|
| | Δx = 25 m | Δx = 100 m | Δx = 25 m | Δx = 100 m |
| $P'_{max}$ [hPa] | 2.0 | 1.7 | 1.9 | 1.6 |
| $P'_{min}$ [hPa] | -5.6 | -5.5 | -5.8 | -5.6 |
| $W_{max}$ [m/s] | 12.7 | 13.6 | 13.1 | 12.9 |
| $W_{min}$ [m/s] | -15.8 | -15.9 | -15.9 | -15.5 |

**The spatial distribution and magnitude of extreme values of the pressure perturbation and W are similar in both CE-C and COSMO-RK solutions.**

# Linear gravity wave: short channel

Skamarock W. C. and J. B. Klemp : Efficiency and Accuracy of the Klemp-Wilhelmson Time-Splitting Technique *MWR*, vol. **122**, 1994.

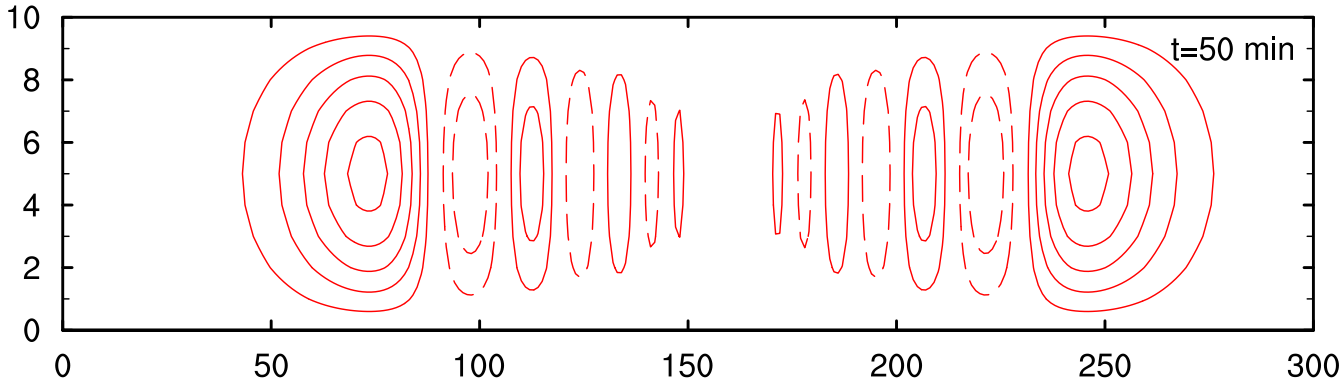


Analytical solution - potential temperature perturbation at t=50 min

**Short channel :**

- Dry flow
- 2-D domain (XZ)
- Periodic b.c. in X
- Domain size 300 km x 10 km
- Free-slip upper and bottom b.c.
- $N_{B\text{-}V} = 0.01\ s^{-1}$
- Ambient flow U= 20 m/s
- The inertia-gravity waves are excited by an initial $\Theta$ perturbation (warm bubble) of small amplitude $\Delta\Theta_0 = 10^{-2}$ K
- Coriolis force acts on the ambient flow perturbation
- Integration time equals 50 minutes
- Isotropic grid ($\Delta x = \Delta z = 1$ km)

# Linear gravity wave: short channel

CE-C Impl.

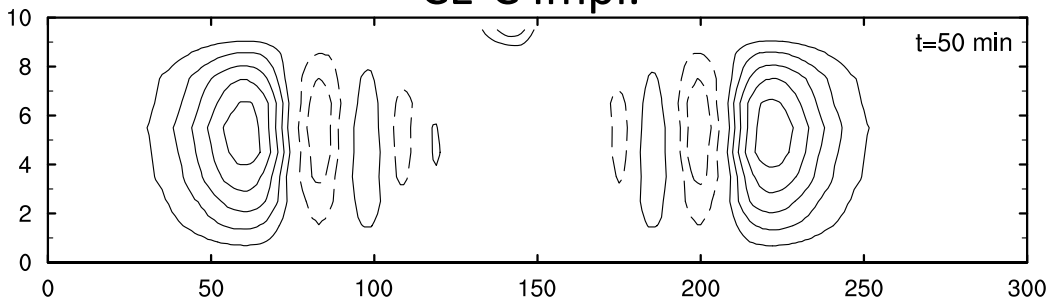


Δx=Δz=1km

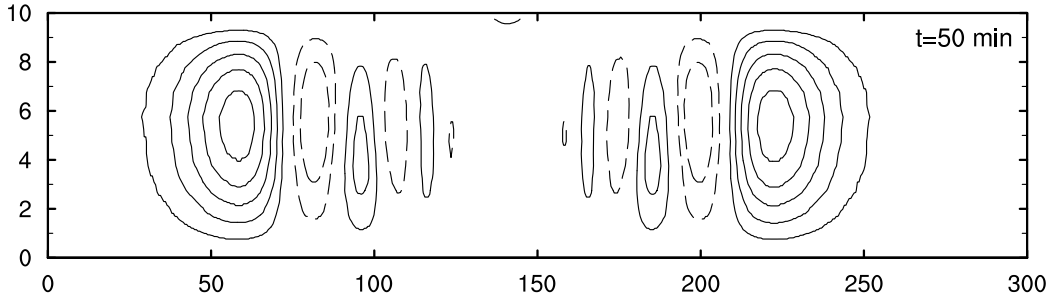


Δx=Δz=0.5km

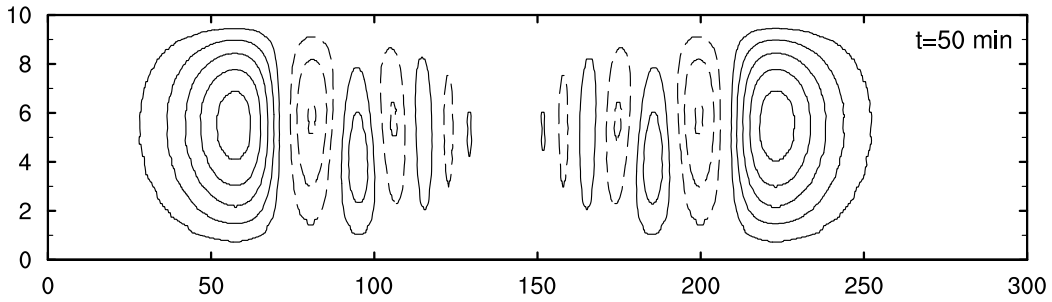


Δx=Δz=0.25km

COSMO RK

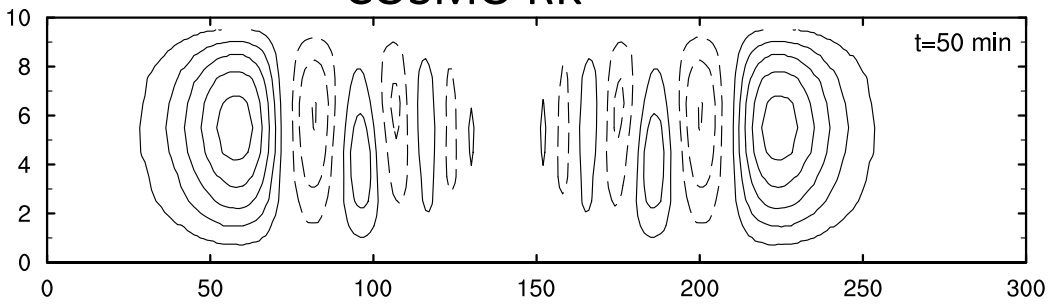


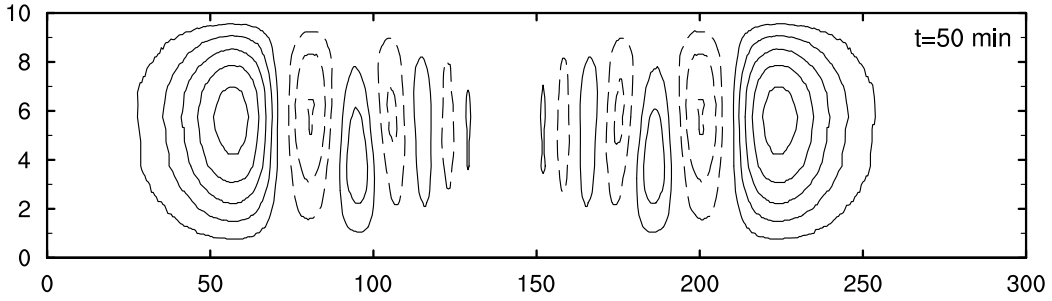


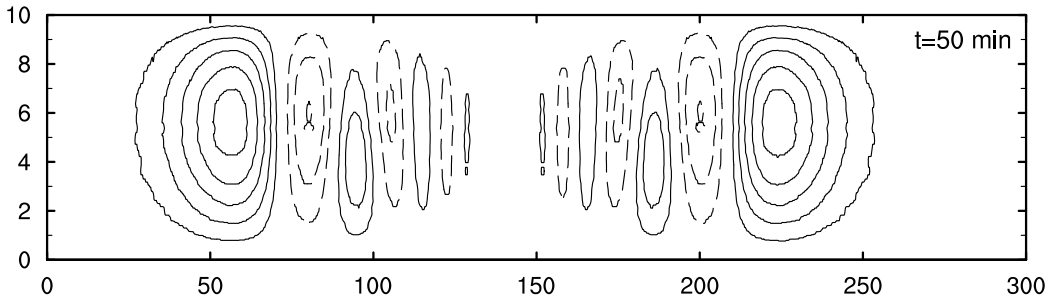


The figures show spatial distribution of the potential temperature perturbation.

# Linear gravity wave: short channel

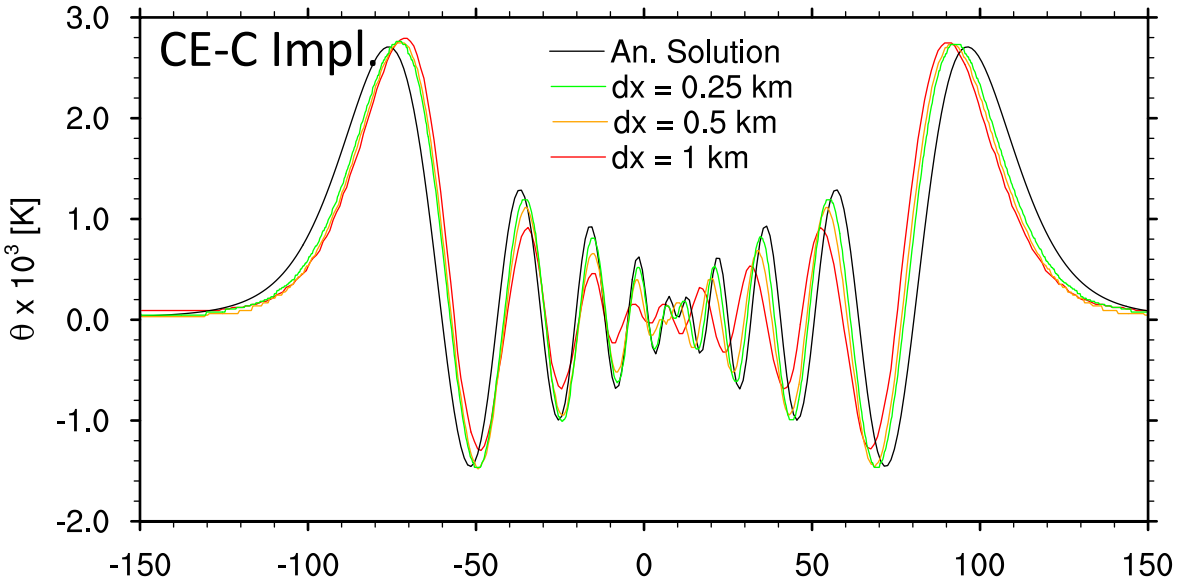


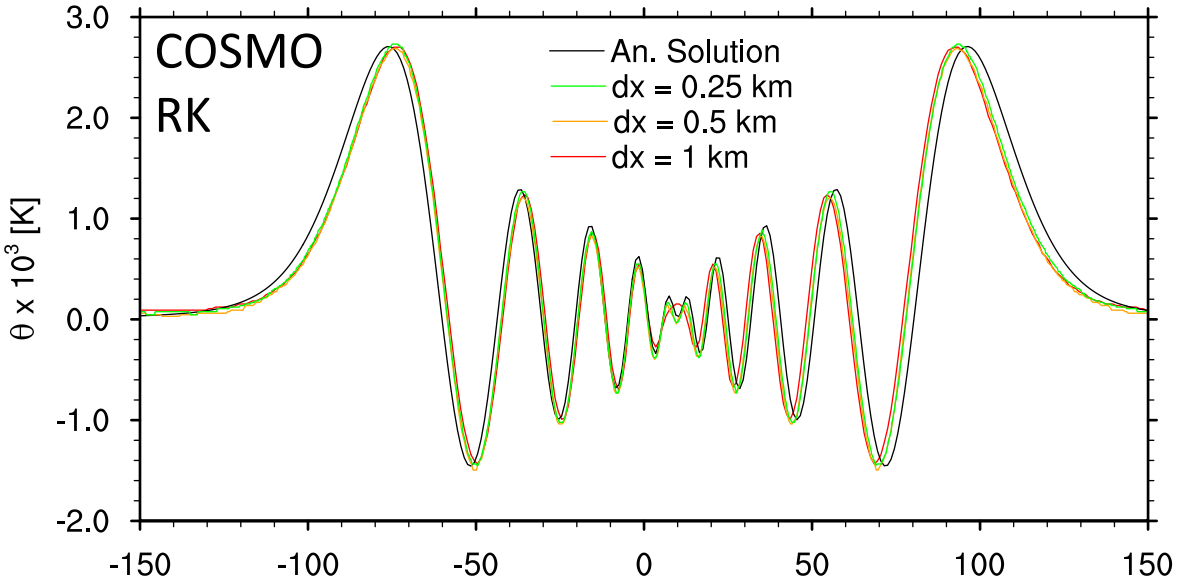


Profiles of potential temperature perturbation θ’ along 5000 m height.

Analytical solution - black line

The numerical solutions (color lines) converge to the analytical formula as the grid spacing in the horizontal and vertical directions decreases.

# Linear gravity wave: long channel

Skamarock W. C. and J. B. Klemp : Efficiency and Accuracy of the Klemp-Wilhelmson Time-Splitting Technique *MWR*, vol. **122**, 1994.

**Long channel :**

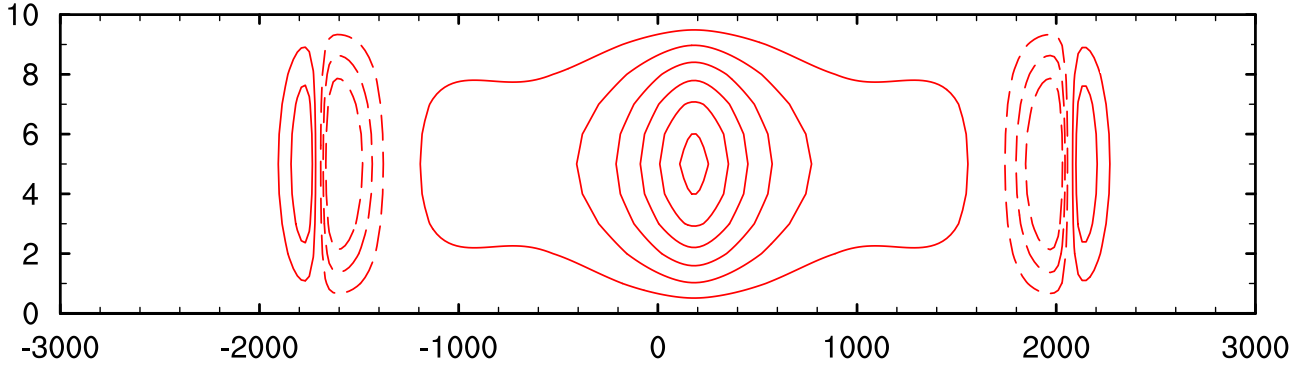


Analytical solution at t=16h 40min

- Dry flow
- 2-D domain (XZ)
- Periodic b.c. in X
- Domain size 6 000 km x 10 km
- Free-slip upper and bottom b.c.
- $N_{B\text{-}V} = 0.01\ s^{-1}$
- Perturbation of the order of $\Delta\Theta_0 = 10^{-2}$ K leads to development of inertia-gravity waves
- Ambient flow U= 20 m/s
- Coriolis force acts on the ambient flow perturbation
- Integration time equals 16 hours 40 minutes
- Non-isotropic grid ($\Delta x$= 20km, $\Delta z$=1 km)

# Linear gravity wave: long channel

CE-C Impl.

COSMO RK

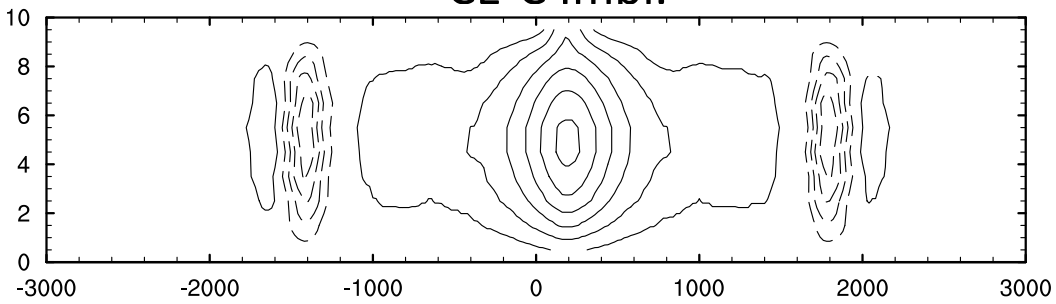


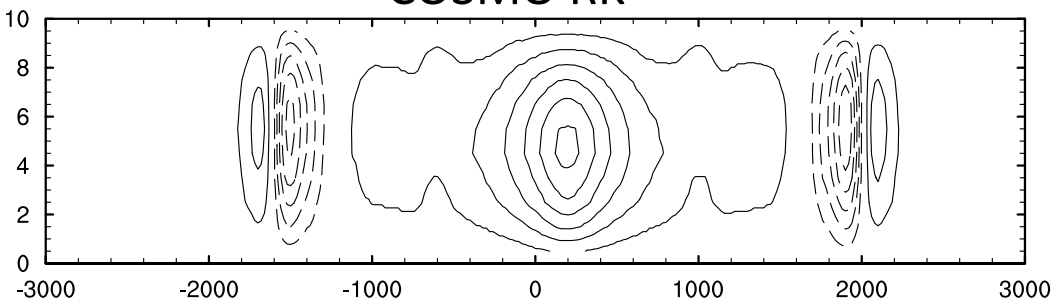


Δx=20km

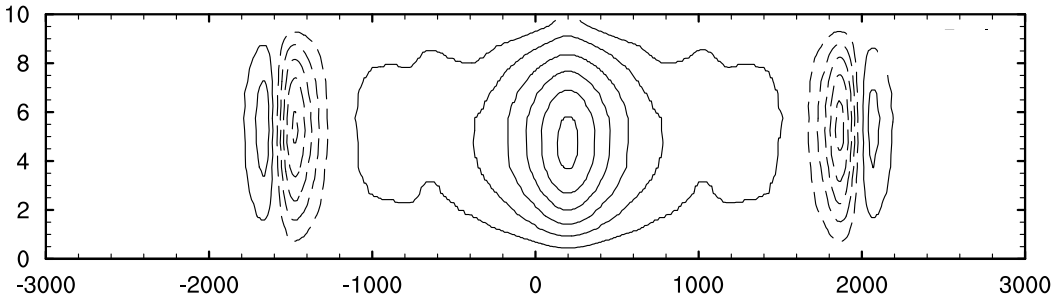


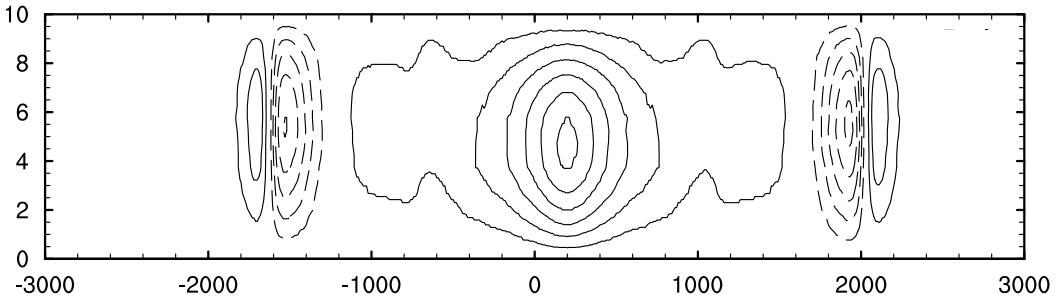


Δx=10km

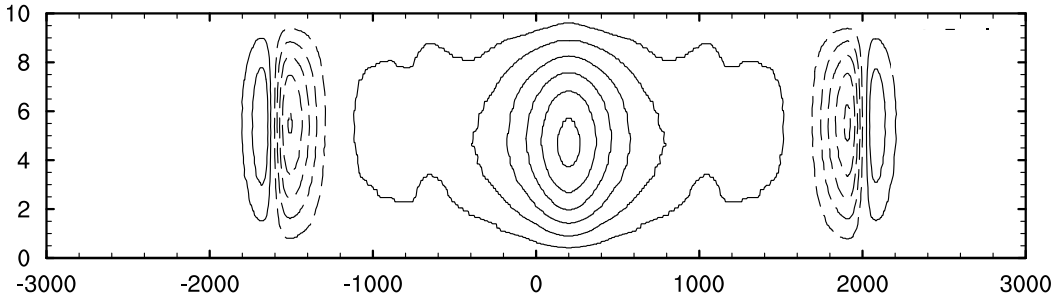


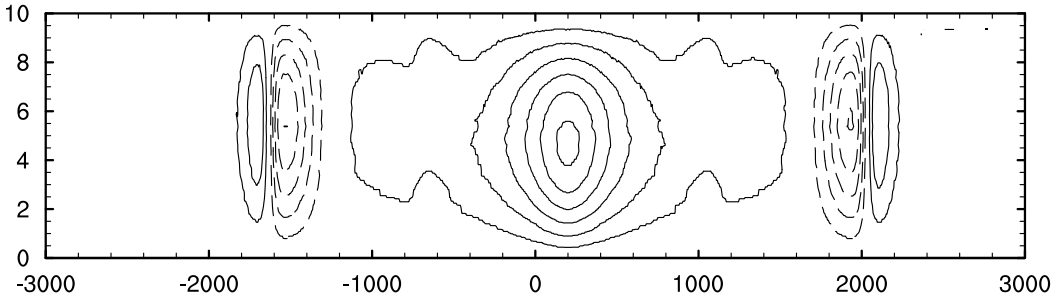


Δx=5km

The figures show spatial distribution of the potential temperature perturbation.

# Linear gravity wave: long channel

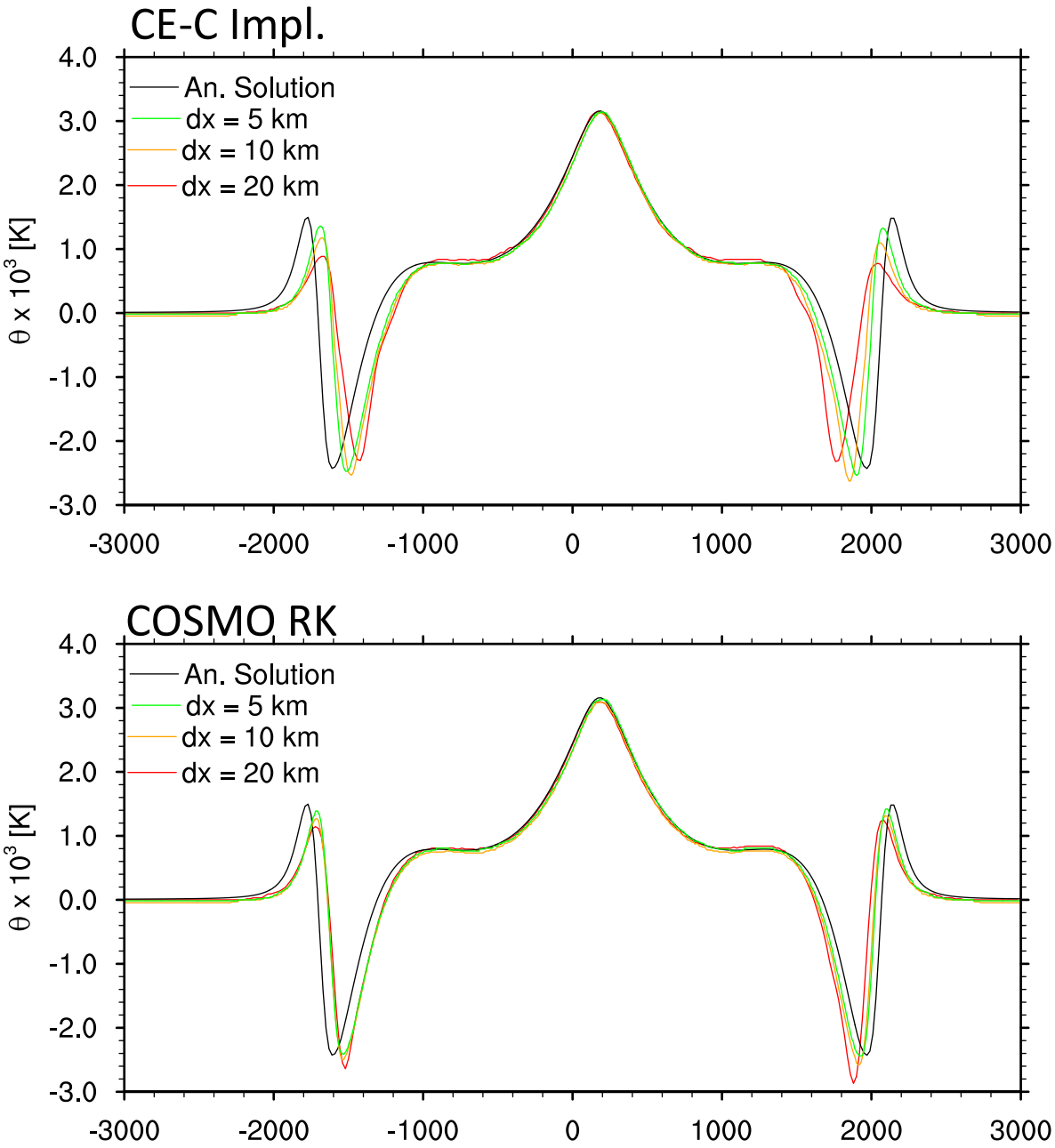


The numerical solutions obtained with both CE-C and C-RK converge to the analytical formula when the the grid resolution increases.

# Testing: Dry orographic flows

## Linear hydrostatic flow :

- $\Delta x$ = 3km, $\Delta z$ = 250 m
- $h_0$ = 1m, a = 16km
- U = 32 m/s
- N = 0.0187 $s^{-1}$

## Nonlinear hydrostatic flow :

- $\Delta x$ = 2.8km, $\Delta z$ = 200 m
- $h_0$ = 800m, a = 16km
- U = 32 m/s
- N = 0.02 $s^{-1}$

## Linear nonhydrostatic flow :

- $\Delta x$ = 0.1km, $\Delta z$ = 250 m
- $h_0$ = 100m, a = 0.5km
- U = 14 m/s
- N = 0.0187 $s^{-1}$

## Nonlinear nonhydrostatic flow :

- $\Delta x$ = 0.2km, $\Delta z$ = 100 m
- $h_0$ = 900m, a = 1km
- U = 13.28 m/s
- N = 0.02 $s^{-1}$


Klemp, J. B. and D. K. Lilly : Numerical Simulation of Hydrostatic Mountain Waves, *JAS*, vol. 35, 1977.

Bonaventura L. : A semi-implicit semi-Lagrangian scheme using the height coordinate for a nonhydrostatic and fully elastic model of atmospheric flows, JCP, vol. 158, 2000.

Pinty, J.P., R. Benoit, E. Richard, and R. Laprise : Simple tests of a semi-implicit semi-Lagrangian model on 2D mountain wave problems, MWR, vol. 123, 1995.

# Linear hydrostatic flow

**Linear hydrostatic flow :**

- **$\Delta x$ = 3km, $\Delta z$ = 250 m**
- **$h_0$ = 1m, a = 16km**
- **U = 32 m/s**
- **N = 0.0187 $s^{-1}$**


Klemp, J. B. and D. K. Lilly : Numerical Simulation of Hydrostatic Mountain Waves, *JAS*, vol. 35, 1977.

Bonaventura L. : A semi-implicit semi-Lagrangian scheme using the height coordinate for a nonhydrostatic and fully elastic model of atmospheric flows, JCP, vol. 158, 2000.

Pinty, J.P., R. Benoit, E. Richard, and R. Laprise : Simple tests of a semi-implicit semi-Lagrangian model on 2D mountain wave problems, MWR, vol. 123, 1995.

# Linear hydrostatic flow : U’ after 11.1 h.

**CE-C Implicit**

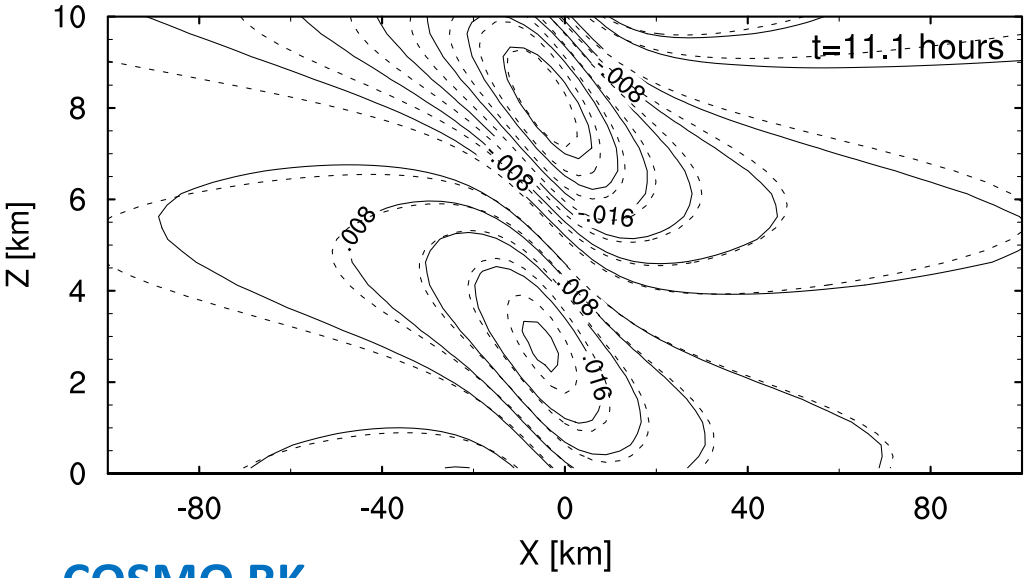


**CE-C Explicit**

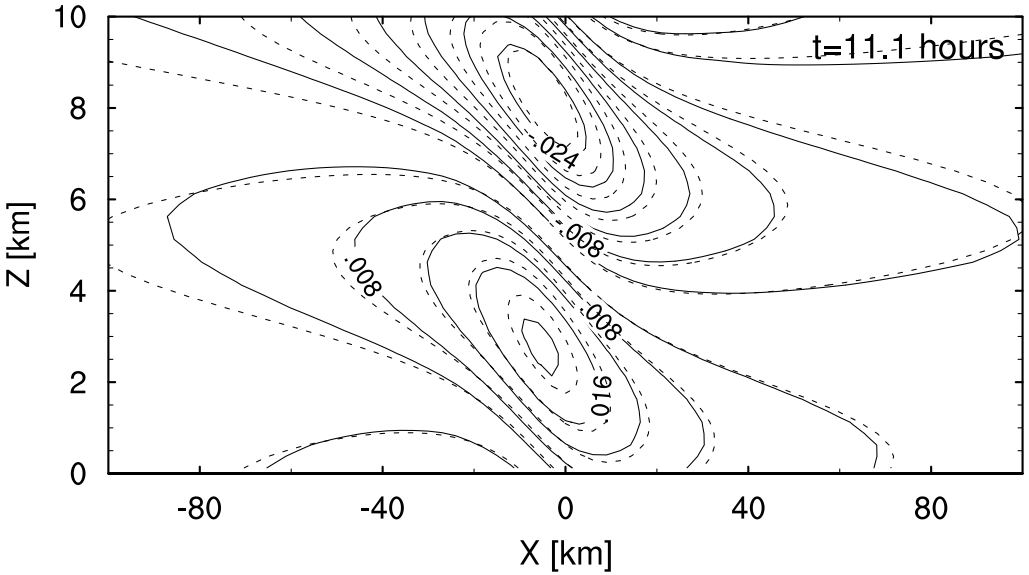


**COSMO RK**

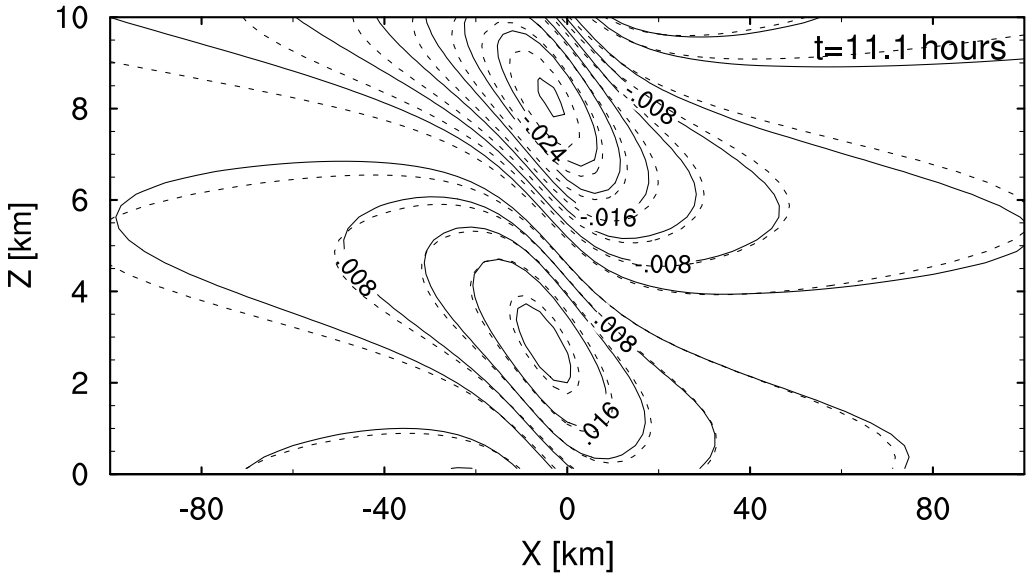


Solid lines – perturbation of U component of velocity computed using different numerical models /approaches.

The plots confirm consistency between numerical solutions and the analytical formula from Klemp et. al.(1977; dashed lines).

# Linear hydrostatic flow : P’ after 11.1 h.

**CE-C Implicit**

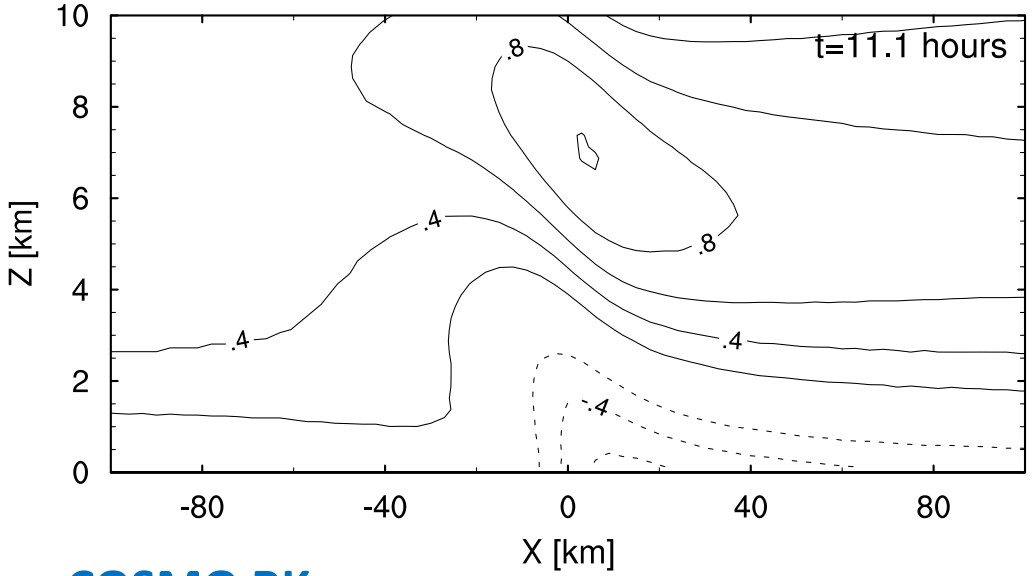


**CE-C Explicit**

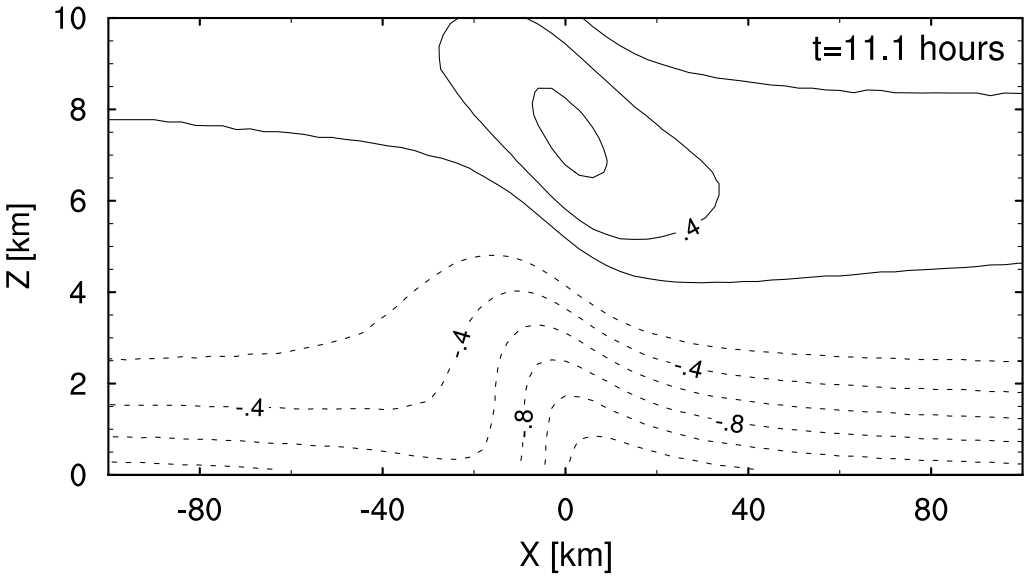


**COSMO RK**

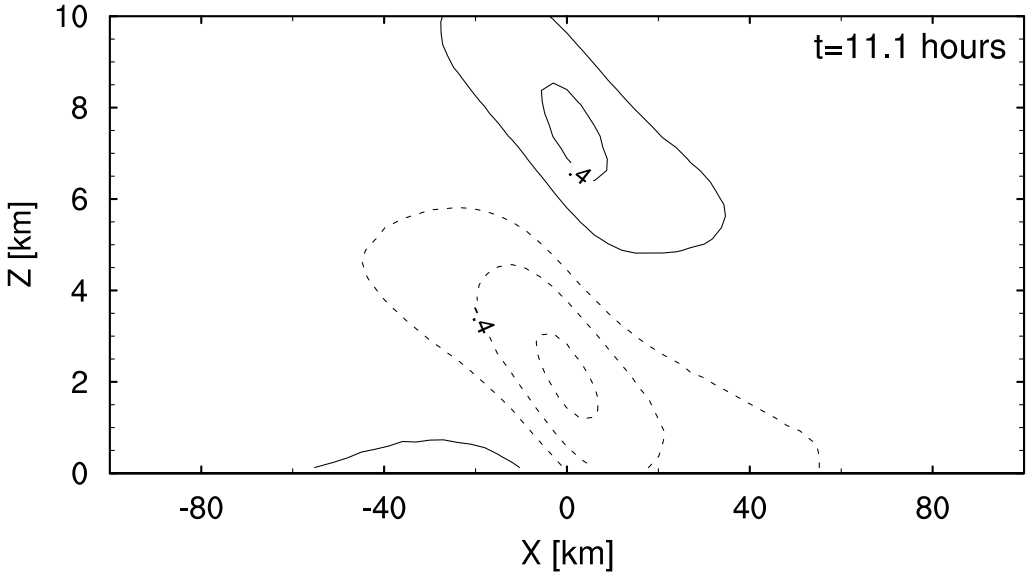


| | $P'_{min}$ [Pa] | $P'_{max}$ [Pa] |
|---|---|---|
| COSMO RK | -0.66 | 0.44 |
| CE-C Expl. | -1.38 | 0.64 |
| CE-C Impl. | -0.65 | 1.00 |

Close to the ground the pressure distribution is different in the solutions obtained with CE-C (both implicit and explicit) and RK.
The reason is not yet fully understood.

# Nonlinear hydrostatic flow

**Nonlinear hydrostatic flow :**

- **$\Delta x$ = 2.8km, $\Delta z$ = 200 m**
- **$h_0$ = 800m, a = 16km**
- **U = 32 m/s**
- **N = 0.02 $s^{-1}$**


Klemp, J. B. and D. K. Lilly : Numerical Simulation of Hydrostatic Mountain Waves, *JAS*, vol. 35, 1977.

Bonaventura L. : A semi-implicit semi-Lagrangian scheme using the height coordinate for a nonhydrostatic and fully elastic model of atmospheric flows, JCP, vol. 158, 2000.

Pinty, J.P., R. Benoit, E. Richard, and R. Laprise : Simple tests of a semi-implicit semi-Lagrangian model on 2D mountain wave problems, MWR, vol. 123, 1995.

# Nonlinear hydrost. flow : U’ after 23.9 h.

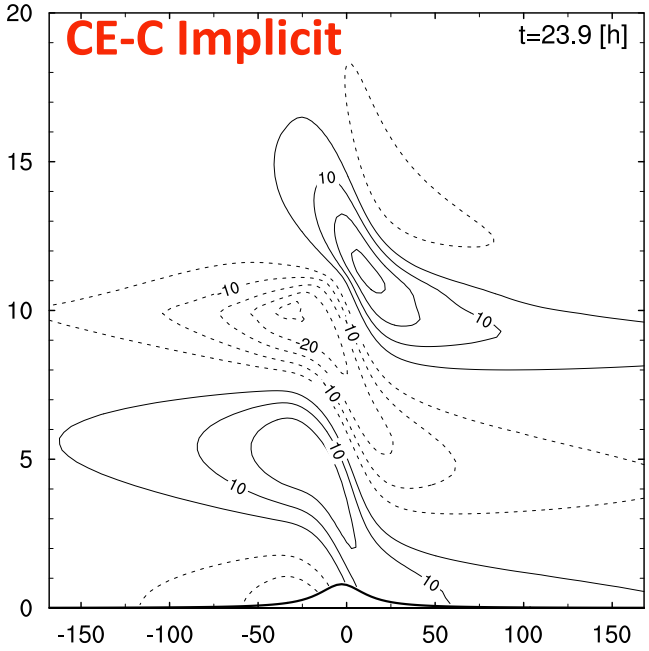


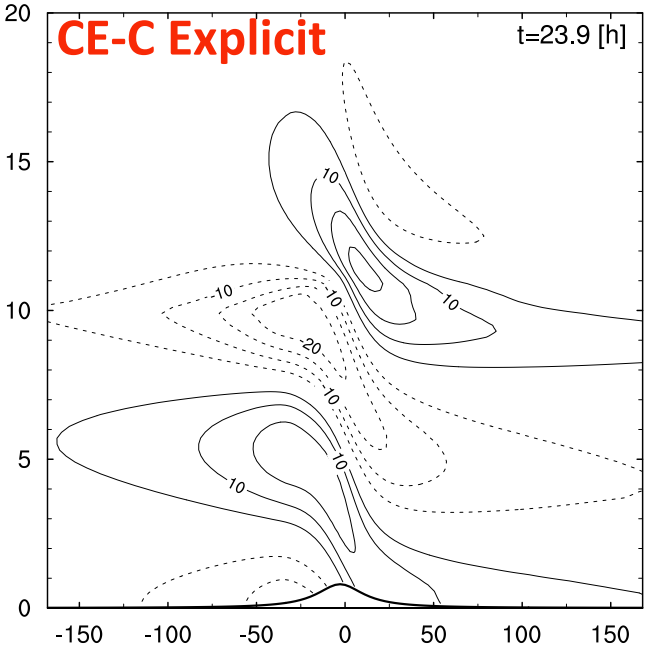


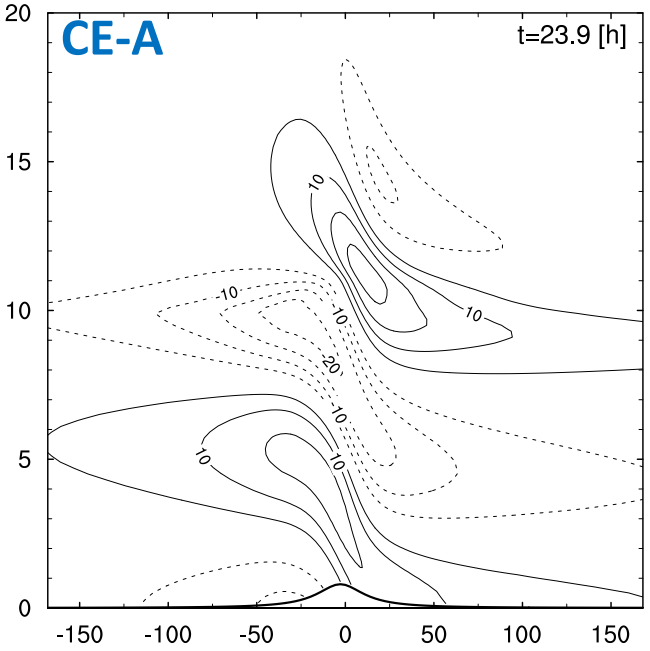


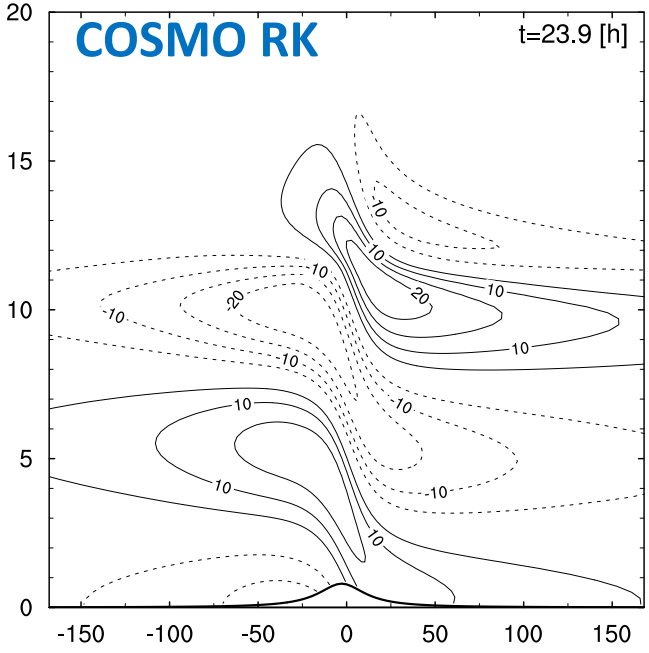


The series of figures present U component of velocity (perturbation). The simulations have been performed using different numerical approaches and different codes.

All solutions are in good quantitative agreement, nevertheless, several small–scale differences are still observed.

The differences in the stratosphere may result from different configuration of the sponge layer.

# Nonlinear hydrost. flow : P’ after 23.9 h.

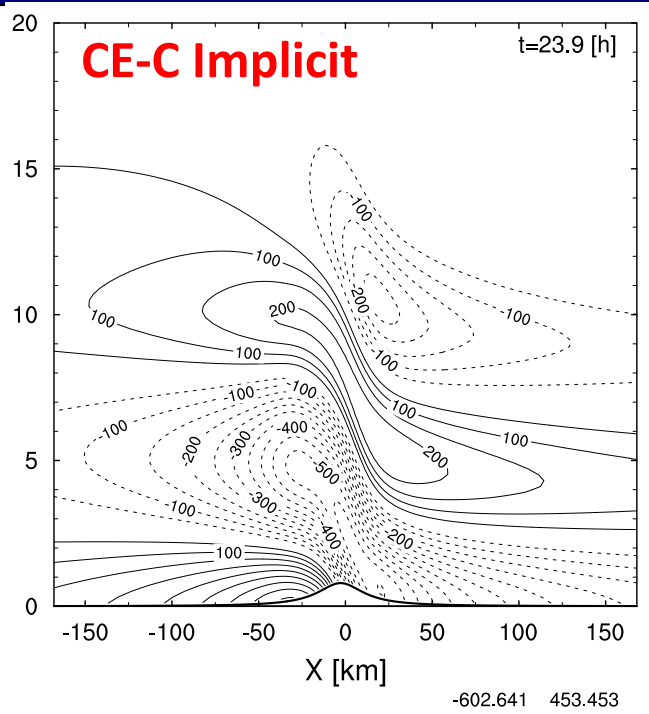


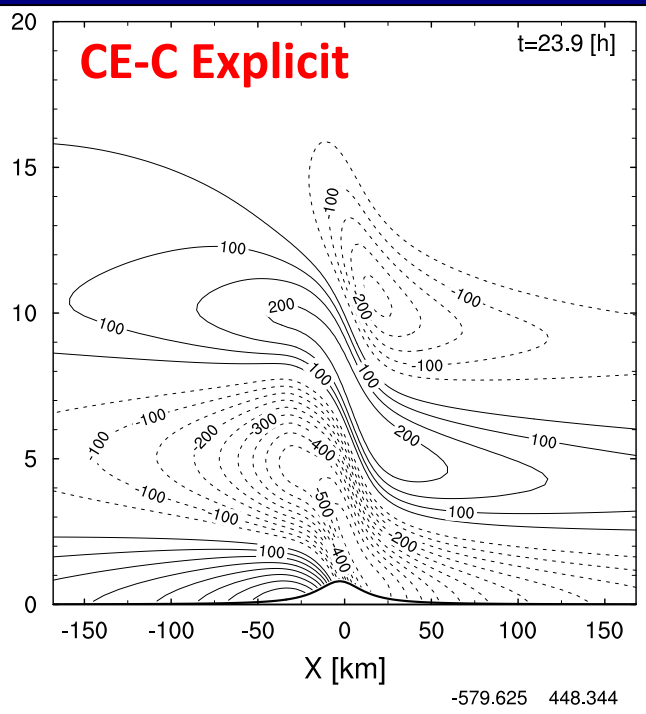


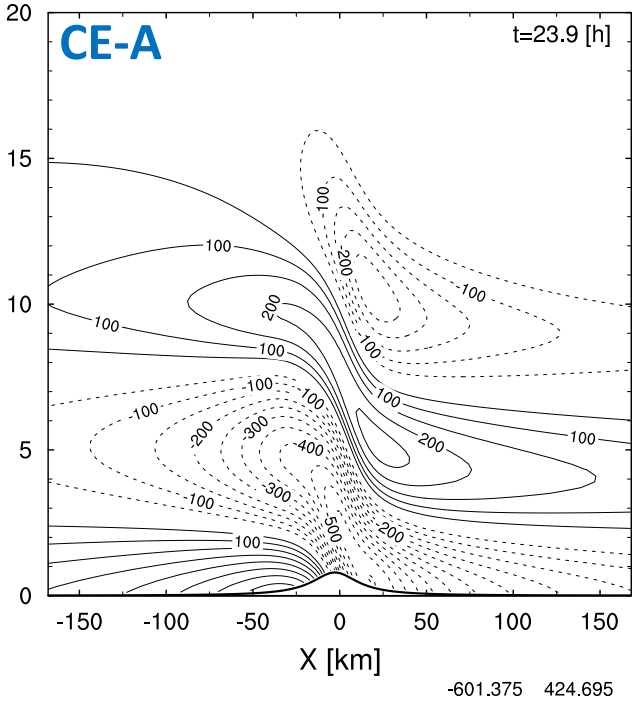


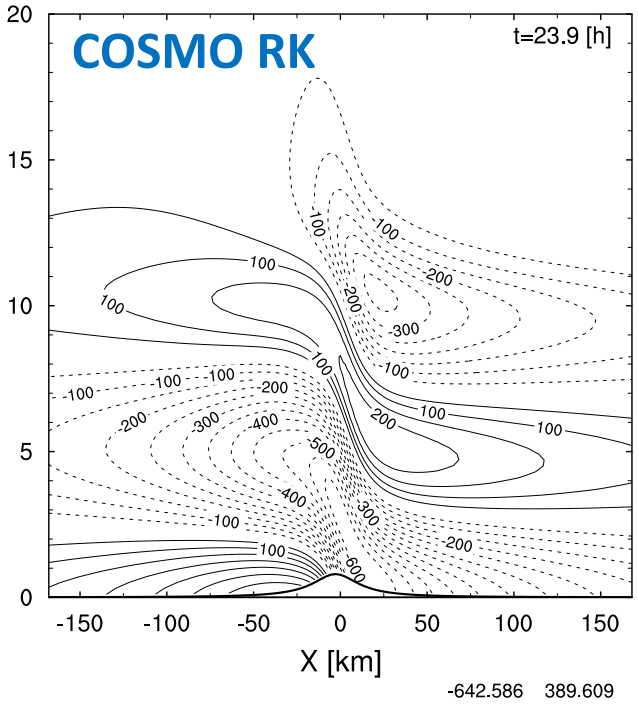


| | $P'_{min}$ [hPa] | $P'_{max}$ [hPa] |
|---|---|---|
| COSMO RK | -6.4 | 3.9 |
| CE-A | -6.0 | 4.2 |
| CE-C Expl. | -5.8 | 4.5 |
| CE-C Impl. | -6.0 | 4.5 |

The differences between extrema are of the order of 0.5 hPa.

# Linear nonhydrostatic flow

**Linear nonhydrostatic flow :**

- **$\Delta x$ = 0.1km, $\Delta z$ = 250 m**
- **$h_0$ = 100m, a = 0.5km**
- **U = 14 m/s**
- **N = 0.0187 $s^{-1}$**


Klemp, J. B. and D. K. Lilly : Numerical Simulation of Hydrostatic Mountain Waves, *JAS*, vol. 35, 1977.

Bonaventura L. : A semi-implicit semi-Lagrangian scheme using the height coordinate for a nonhydrostatic and fully elastic model of atmospheric flows, JCP, vol. 158, 2000.

Pinty, J.P., R. Benoit, E. Richard, and R. Laprise : Simple tests of a semi-implicit semi-Lagrangian model on 2D mountain wave problems, MWR, vol. 123, 1995.

# Linear nonh. flow : P’ after 80 min.

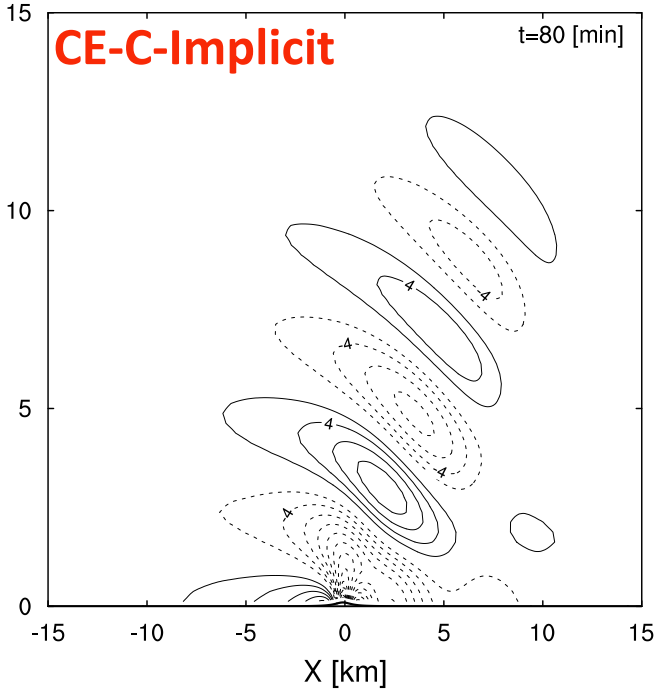


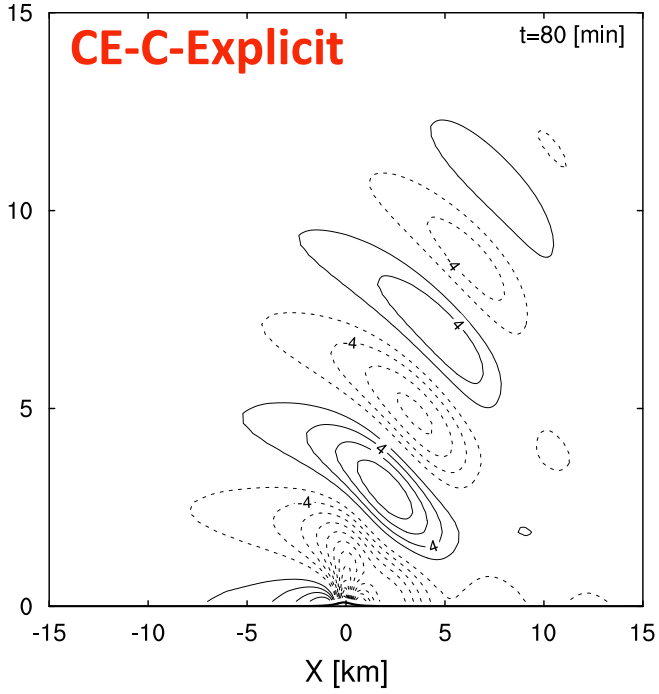


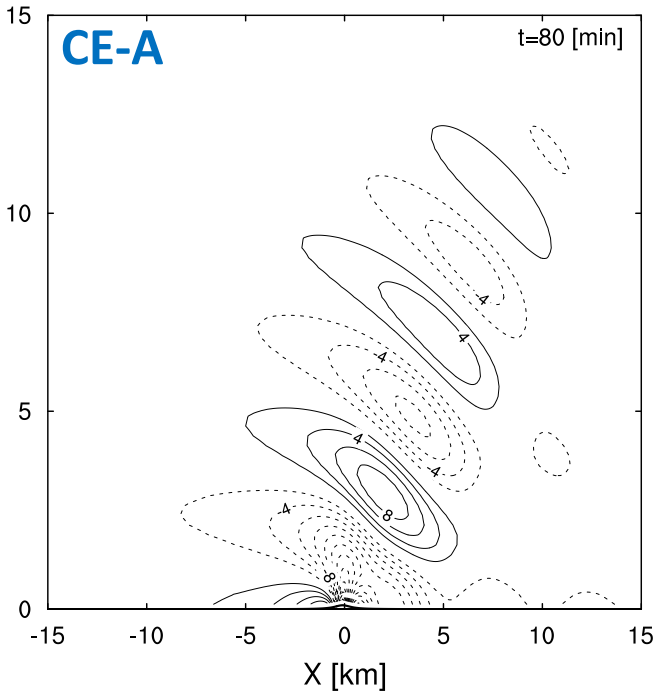


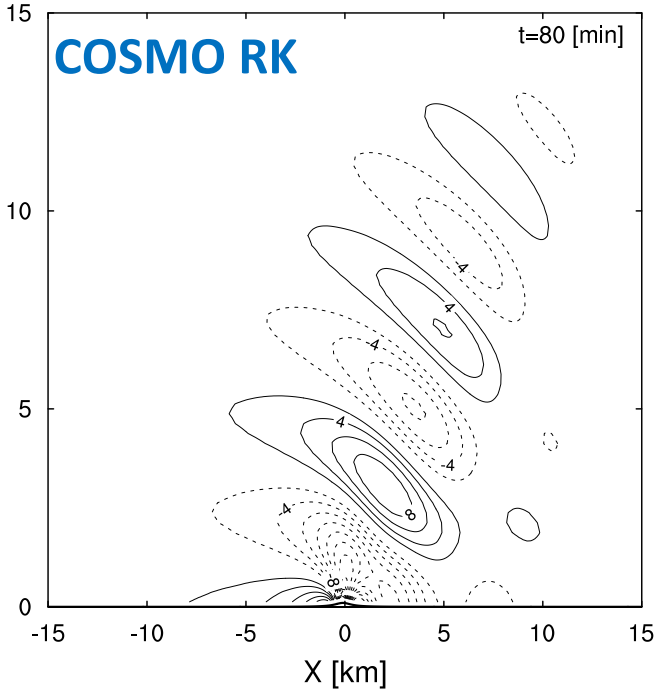


| | $P'_{min}$ [Pa] | $P'_{max}$ [Pa] |
|---|---|---|
| COSMO RK | -29.9 | 10.9 |
| CE-A | -29.2 | 9.6 |
| CE-C Expl. | -27.2 | 9.9 |
| CE-C Impl. | -28.1 | 10.1 |

The results are in good qualitative and quantitative agreement.

# Nonlinear nonhydrostatic flow

**Nonlinear nonhydrostatic flow :**

- **$\Delta x = 0.2$km, $\Delta z = 100$ m**
- **$h_0 = 900$m, $a = 1$km**
- **$U = 13.28$ m/s**
- **$N = 0.02$ $s^{-1}$**


Klemp, J. B. and D. K. Lilly : Numerical Simulation of Hydrostatic Mountain Waves, *JAS*, vol. 35, 1977.

Bonaventura L. : A semi-implicit semi-Lagrangian scheme using the height coordinate for a nonhydrostatic and fully elastic model of atmospheric flows, JCP, vol. 158, 2000.

Pinty, J.P., R. Benoit, E. Richard, and R. Laprise : Simple tests of a semi-implicit semi-Lagrangian model on 2D mountain wave problems, MWR, vol. 123, 1995.

# Nonlinear nonh. flow : P’ after 40 min.

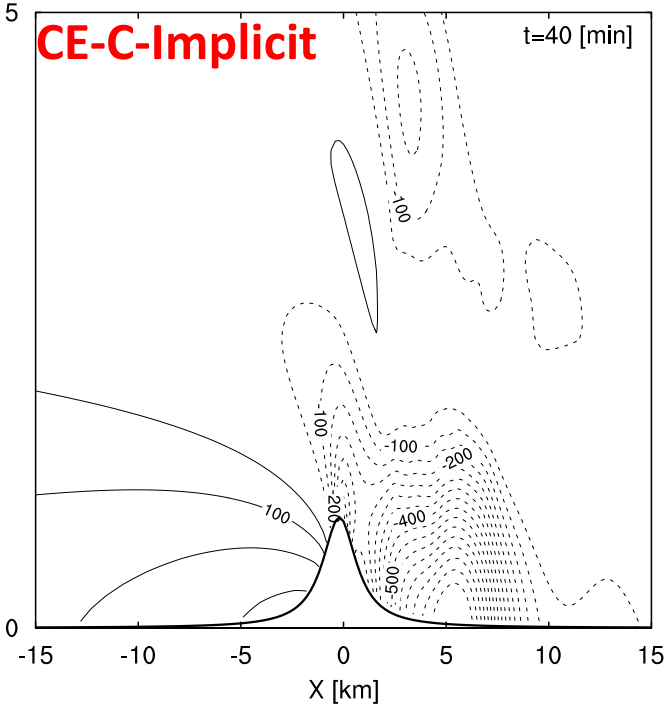


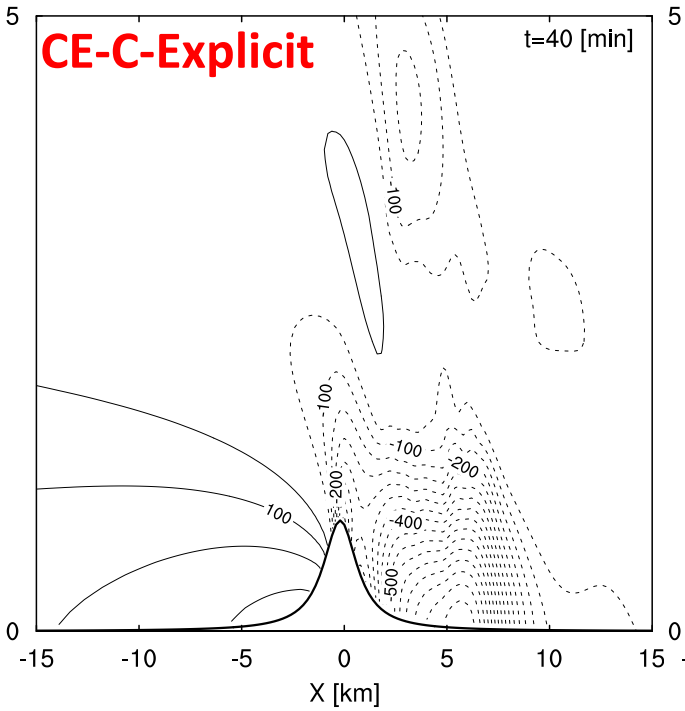


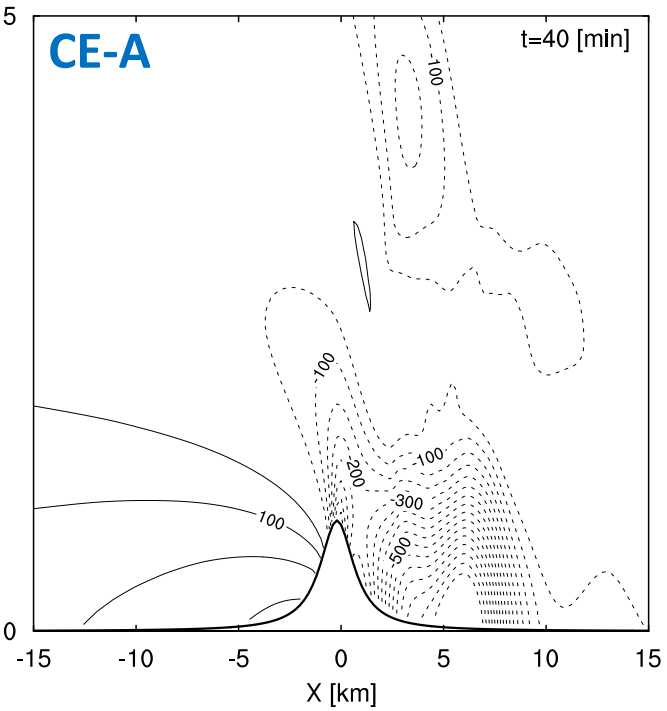


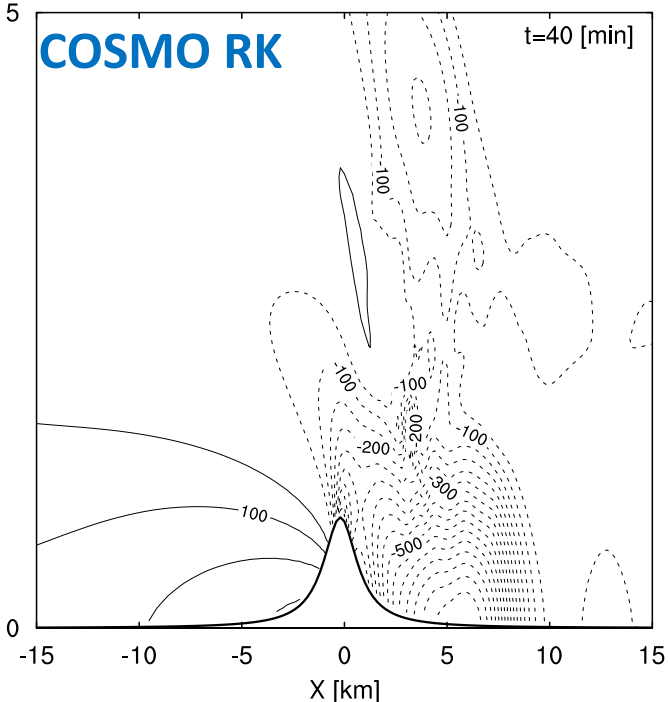


| | $P'_{min}$ [hPa] | $P'_{max}$ [hPa] |
|---|---|---|
| COSMO RK | -8.5 | 2.0 |
| CE-A | -9.5 | 2.1 |
| CE-C-Expl. | -8.4 | 2.2 |
| CE-C-Impl. | -8.8 | 2.2 |

The plots reveal high consistency between solutions obtained with different numerical models. Both the pressure distribution and the extreme values are similar in all 4 simulations.

# Summary

- The anelastic COSMO-EULAG model is capable to provide competitive weather forecasts (in simulations without data assimilation).
- It can be utilized for high resolution simulations over steep terrain.
- The most recent version of COSMO-EULAG with the compressible dynamical core (CE-C) has been tested in a set of benchmark idealized experiments.
- In general the results obtained with CE-C are in good agreement with the reference solutions.
- The following research is going to be focused on pressure recovery, forecast verification, tuning and improving numerical performance (e.g. single/double precision) of CE-C model